Journal of Cosmology
and Astroparticle
Physics

SISSA

PAPER • OPEN ACCESS

Stairway to axions: the cross-correlation of birefringence and galaxies from NPIPE and Quaia

To cite this article: S. Arcari *et al* JCAP06(2026)015

View the article online for updates and enhancements.

You may also like

- Commutative and non-commutative signatures of anisotropic inflation: constraints from planck PR4 data
Akash Gandhi
- Full-sky Models of Galactic Microwave Emission and Polarization at Subarcminute Scales for the Python Sky Model
The Pan-Experiment Galactic Science Group, Julian Borrill, Susan E. Clark et al.
- Planck PR4 (NPIPE) map-space cosmic birefringence
Raelyn M. Sullivan, Arefe Abghari, Patricia Diego-Palazuelos et al.

This content was downloaded from IP address 5.90.140.123 on 04/06/2026 at 17:19

Journal of Cosmology and Astroparticle Physics
An IOP and SISSA journal

Received: October 6, 2025
Accepted: April 20, 2026
Published: June 4, 2026

Stairway to axions: the cross-correlation of birefringence and galaxies from NPIPE and Quaia

S. Arcari,[a,b] **N. Bartolo**,[c,d,e] **G. Fabbian**,[f,g] **A. Greco**,[h] **A. Gruppuso**,[i,j,a] **M. Lattanzi**,[a,b] **P. Natoli**,[a,b] **L. Pagano**[a,b] **and G. Zagatti**[a,b]

[a] *Dipartimento di Fisica e Scienze della Terra, Università degli Studi di Ferrara, Via G. Saragat 1, I-44122 Ferrara, Italy*
[b] *Istituto Nazionale di Fisica Nucleare, Sezione di Ferrara, Via G. Saragat 1, I-44122 Ferrara, Italy*
[c] *Dipartimento di Fisica e Astronomia "Galileo Galilei", Universià degli Studi di Padova, Via Marzolo 8, I-35131 Padova, Italy*
[d] *Istituto Nazionale di Fisica Nucleare, Sezione di Padova, Via Marzolo 8, I-35131 Padova, Italy*
[e] *Istituto Nazionale di Astrofisica — Osservatorio Astronomico di Padova, Vicolo dell'Osservatorio 5, I-35122 Padova, Italy*
[f] *Kavli Institute for Cosmology Cambridge, Madingley Road, Cambridge CB3 0HA, U.K.*
[g] *Institute of Astronomy, Madingley Road, Cambridge CB3 0HA, U.K.*
[h] *Department of Astronomy, University of Florida, 211 Bryant Space Science Center, Gainesville, FL 32611, U.S.A.*
[i] *Istituto Nazionale di Astrofisica — Osservatorio di Astrofisica e Scienza dello Spazio di Bologna, Via Gobetti 101, I-40129 Bologna, Italy*
[j] *Istituto Nazionale di Fisica Nucleare, Sezione di Bologna, Viale Berti Pichat 6/2, I-40127 Bologna, Italy*

E-mail: stefano.arcari@unife.it, nicola.bartolo@pd.infn.it, fabbiang@cardiff.ac.uk, alessandro.greco@ufl.edu, alessandro.gruppuso@inaf.it, massimiliano.lattanzi@fe.infn.it, paolo.natoli@unife.it, luca.pagano@unife.it, giorgia.zagatti@unife.it

Abstract: We present the first measurement of the cross-correlation between anisotropic birefringence and galaxy number counts, utilizing polarization data from *Planck* NPIPE and the Quaia quasar catalog. By employing a QML/pseudo-C_ℓ combined estimator, we compute the angular power spectrum up to $\ell = 191$ from birefringence and clustering maps at $N_{\rm side} = 64$. Our analysis indicates that the observed spectrum is well consistent with the null-hypothesis, with a probability to exceed of 37% and an estimated scale-invariant amplitude of $A^{\mathcal{D}_\ell} = (2.22 \pm 2.09) \times 10^{-4}\,\mathrm{deg}$, at the 68% confidence level. Finally, we derive constraints on the axion-parameters within an early dark energy model of birefringence. Our

© 2026 The Author(s). Published by IOP Publishing Ltd on behalf of Sissa Medialab. Original content from this work may be used under the terms of the Creative Commons Attribution 4.0 licence. Any further distribution of this work must maintain attribution to the author(s) and the title of the work, journal citation and DOI.

https://doi.org/10.1088/1475-7516/2026/06/015

JCAP06(2026)015

findings reach 95% upper limits of up to $10^{-14}\,\mathrm{GeV}^{-1}$ on the axion-photon coupling, for the misalignment angle condition $|\theta_i|/\pi \geq 0.7$. For masses around $10^{-32}\,\mathrm{eV}$ and high initial misalignment angles, i.e. $|\theta_i|/\pi \geq 0.99$, we obtain an unprecedented upper bound on the axion-photon coupling down to $g_{\phi\gamma} = 10^{-15}\,\mathrm{GeV}^{-1}$. This result opens a previously unexplored window in parameter space, providing the first constraint in this ultra-light mass regime.

Keywords: axions, CMBR polarisation, galaxy clustering

ArXiv ePrint: 2509.22273

JCAP06(2026)015

Contents

1 Introduction **1**

2 Theoretical model **2**

3 Datasets **4**
3.1 *Planck* NPIPE 4
3.2 Quaia 5

4 Methodology **6**
4.1 Power spectrum estimation 6
4.2 Covariance estimation 8

5 Results **9**
5.1 The measured cross-correlation 10
5.2 Scale invariant amplitude 11
5.3 Bound on axion-photon coupling 13

6 Conclusion **15**

A Impact of binning and galaxy bias model **17**

B Galaxy distribution vs. scalar field evolution **20**

JCAP06(2026)015

1 Introduction

The Cosmic Microwave Background (CMB) is a pivotal tool for exploring the early universe and fundamental cosmology. Initial CMB experiments [1–3], including the *Planck* satellite [4–7], focused on temperature anisotropies, confirming the standard cosmological model while revealing subtle anomalies. Recently, research has shifted towards CMB polarization, which provides deeper insights into cosmic inflation, parity violation, and the early universe's dynamics. By analyzing these polarization patterns, researchers can place constraints on new physics parameters, providing insights into phenomena beyond the standard cosmological model, including dark matter, dark energy, and other exotic fields.

A notable effect in CMB studies is cosmic birefringence (CB) [8–24], the rotation of the linear polarization plane of CMB radiation. A well-known modification of the standard model involves adding a Chern-Simons term to the Maxwell Lagrangian density, which describes an interaction between photons and a new scalar field ϕ [8–13]:

$$\mathcal{L} \supset -\frac{1}{2}\, g^{\mu\nu}\partial_\mu\phi\,\partial_\nu\phi - V(\phi) - \frac{1}{4}\, g_{\phi\gamma}\,\phi\, F_{\mu\nu}\tilde{F}^{\mu\nu}\,, \tag{1.1}$$

where $g^{\mu\nu}$ is the metric tensor, $V(\phi)$ the field potential, $g_{\phi\gamma}$ the field-to-photon coupling, and $\tilde{F}^{\mu\nu} = \epsilon^{\mu\nu\rho\sigma}F_{\rho\sigma}/2$ the Hodge dual of the Maxwell tensor $F_{\mu\nu}$. The last term of eq. (1.1) induces parity violation when the field ϕ retains spacetime dependence, and appears naturally

for axion-like particles (ALPs) [15–17, 25–56]. The primary effect on CMB is a mixing between E- and B-modes, leading to non vanishing TB and EB cross-correlations. Recent works [19, 57–61] have exploited novel analysis techniques yielding a hint of detection (at 3σ) for the isotropic CB angle. Moreover, one expects anisotropies in the birefringence angle to arise naturally from the fluctuations of the scalar. These variations across the sky have been studied extensively through CMB data [62–66] and proposed as a tool to constrain early dark energy (EDE) models and axions [16, 17, 45, 54, 67].

In this work, we show, for the first time, the cross-correlation between anisotropic birefringence and the spatial distribution of galaxies, as measured by the combination of CMB polarization data from *Planck* PR4 [68, 69] and the all-sky quasar catalog Quaia [70–73]. We exploit a pseudo-C_ℓ approach (supported by QML estimates at low-ℓ's) over maps for anisotropic birefringence derived through the EB-estimator of ref. [66], based on [74, 75], and for galaxy number counts derived from Quaia [70]. The associated covariance is consistently calculated using 400 polarization plus noise simulations from *Planck* NPIPE [68], alongside an equal number of realizations from the quasar catalog. Our results reveal a cross-correlation well consistent with the null-hypothesis across the whole range of multipoles. Finally, we exploit this novel signal to constrain axion-parameters through a Gaussian likelihood approach over theoretical spectra derived with a properly modified version of the Boltzmann code `CLASS` [76, 77]. We introduce an unprecedented upper bound on the axion-photon coupling $g_{\phi\gamma}$ within the ultralight mass range $m_\phi = [10^{-33},\ 10^{-28}]$ eV. In conclusion, we expand on the theoretical introduction of the birefringence-LSS cross-correlation of ref. [54] by measuring it for the first time, and show its exceptional potential in constraining axion-like physics.

The paper is organized as follows: in section 3 we describe the data and simulation sets used to derive the birefringence-galaxy cross-correlation and related covariance, whilst in section 4 we briefly summarize its theoretical interpretation and the adopted estimation techniques. In section 5 we show the measured cross-correlation, alongside our constraints on the axion-photon coupling. Finally, conclusions are drawn in section 6. Appendix A serves as an informative summary of possible implications on the results of changing the multipole-binning scheme.

Throughout the paper, we assume a spatially flat ΛCDM cosmology with cosmological parameters as derived by the final *Planck* data release [69].[1]

2 Theoretical model

In this study, we regard two different probes: the anisotropic birefringence $\alpha(\hat{\mathbf{n}})$ and the spatial distribution of galaxies as measured by the Quaia quasar overdensity $\delta_g(\hat{\mathbf{n}})$. As discussed in section 1, the former can be generated by parity violating couplings of ALPs to the electromagnetic sector, and we expect a non-zero correlation due to both probes being sourced by the metric perturbations and related gravitational potentials [45, 67].[2] This has been extensively studied theoretically in ref. [54] and presented, for the first time, as a

[1] Let us remind that ALPs are an extension of the underlying cosmological model.

[2] The physical mechanism underlying this correlation is that the spatial fluctuations in both the scalar field (and consequently in the birefringence angle) and the galaxy density are sourced by the same underlying metric perturbations.

JCAP06(2026)015

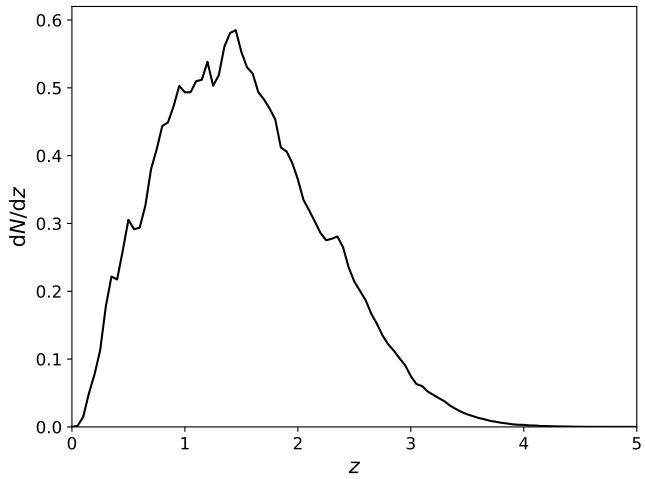


Figure 1. Redshift distribution of sources within the Quaia catalog [70], used as the selection function in eq. (2.3) for the computation of the theoretical cross-correlation. Reproduced from [70]. CC BY 4.0.

valuable tool to explore the axion-parameter space. The angular cross-correlation reads[3]

$$C_\ell^{\alpha g} = 4\pi \int \frac{\mathrm{d}k}{k}\, \mathcal{P}_\mathcal{R}(k) \Delta_\ell^\alpha(k) \Delta_\ell^g(k)\,, \tag{2.1}$$

where $\mathcal{P}_\mathcal{R}$ is the primordial power spectrum, while $\Delta_\ell^\alpha(k)$ and $\Delta_\ell^g(k)$ are the respective kernels for birefringence and galaxies [76, 78, 79]:

$$\Delta_\ell^\alpha(k) = g_{\phi\gamma} \int_0^{\tau_0} \mathrm{d}\tau\; g(\tau) T_{\delta\phi}(\tau,\, k) j_\ell\left[k(\tau_0 - \tau)\right]\,, \tag{2.2}$$

$$\Delta_\ell^g(k) = \int \mathrm{d}z\; \frac{\mathrm{d}N}{\mathrm{d}z} b(z) S_D(z,\, k) j_\ell\left[k\, r(z)\right]\,. \tag{2.3}$$

In eq. (2.2), $g(\tau)$ is the full photon visibility function with respect to conformal time τ, $T_{\delta\phi}(\tau,\, k)$ is a transfer function between the primordial power spectrum $\mathcal{P}_\mathcal{R}(k)$ and that of the field fluctuations $\delta\phi$, and $j_\ell\left[k(\tau_0 - \tau)\right]$ the ℓ-th spherical Bessel function. This kernel is governed by the Klein-Gordon equation of axion-perturbations

$$\delta\phi'' + 2\mathcal{H}\,\delta\phi' + \left(k^2 + a^2 \frac{\mathrm{d}^2 V}{\mathrm{d}\bar{\phi}^2}\right)\delta\phi = -\frac{1}{2} h' \bar{\phi}'\,, \tag{2.4}$$

with $\mathcal{H}$ being the conformal Hubble parameter, a the scale factor, h the metric perturbation in synchronous gauge, $\bar{\phi}$ the background field, and primes denoting derivatives with respect to conformal time τ.[4] For our analysis, we choose an axion-potential V stemming from EDE models of the string axiverse [27, 31, 80]:

$$V(\phi) = m_\phi^2 f_a^2 \left[1 - \cos\frac{\phi}{f_a}\right]^3\,. \tag{2.5}$$

[3]Here, adiabatic initial conditions are assumed.

[4]In eq. (2.4) since h' is multiplied by the background (homogeneous) field derivative, $\bar{\phi}'$, the forcing term is suppressed when the field is frozen, while is large when the field is varying rapidly. The cosmological epoch at which the scalar field begins to evolve from its initial frozen state is determined by its mass: the lighter the mass, the later the field starts its evolution. See also appendix B.

JCAP06(2026)015

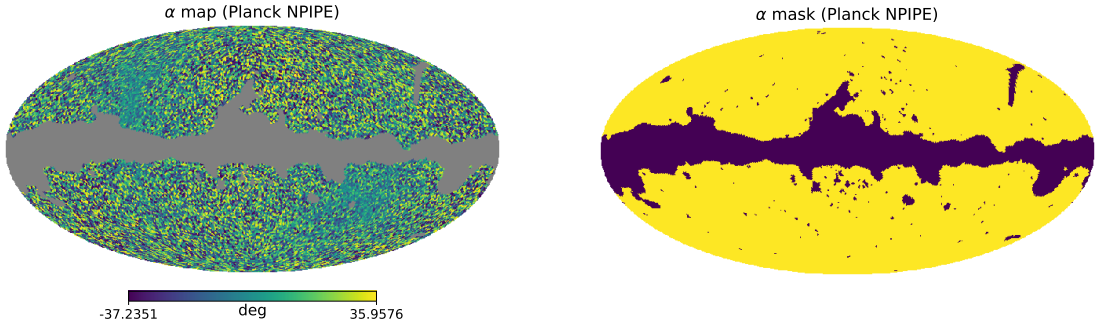


Figure 2. Anisotropic birefringence map derived from *Planck* NPIPE polarization data with the EB-estimator of ref. [66] (*Left*), and corresponding sky mask (*Right*). Reproduced from [66]. CC BY 4.0.

Here, f_a is the scale of the spontaneous breakdown of a continuous symmetry[5] and m_ϕ the axion mass. In summary, the axion evolution and its impact on birefringence will be controlled by the axion-photon coupling $g_{\phi\gamma}$, the axion mass and its initial misalignment $\theta_i = \phi_i/f_a$ (setting the initial condition of the axion field as well[6]).

In eq. (2.3), $\mathrm{d}N(z)/\mathrm{d}z$ is the galaxy redshift distribution, $b(z)$ the linear bias between the galaxy and matter overdensity, S_D a source function related to the growth of structure and the Bardeen potentials, and $r(z)$ the comoving radial distance. The former is taken directly from the data products of Quaia discussed in section 3.2 and shown in figure 1. For the galaxy bias, we follow the prescription of [81]:

$$b(z) = 0.278\left[(1+z)^2 - 6.565\right] + 2.393\,. \tag{2.6}$$

Eq. (2.1) and the aforementioned axion model and clustering ingredients have been implemented in a modified version of the Boltzmann code `CLASS` [77, 82], based on the birefringence implementation of ref. [45] and[7] the galaxy guidelines of `CLASSgal` [76].

3 Datasets

This section serves as a brief description of the data products employed in our study. Specifically, we review the procedure to obtain anisotropic birefringence maps from *Planck* NPIPE [68] and galaxy overdensity maps from Quaia [70].

3.1 *Planck* NPIPE

Cosmic birefringence induces a rotation of linearly polarized light by an angle $\alpha(\hat{\mathbf{n}}) = \bar{\alpha} + \delta\alpha(\hat{\mathbf{n}})$, where the isotropic contribution $\bar{\alpha}$ arises from the background field, while field perturbations induce a dependence on the direction on the sky $\hat{\mathbf{n}}$ in the anisotropic counterpart $\delta\alpha(\hat{\mathbf{n}})$. As a consequence, the observed CMB E- and B-modes are rotated and mixed [83, 84] and inherit information on the rotation field. Harmonic estimators can be exploited to reconstruct

[5] We fix it to the *Planck* mass.

[6] The considered potential arises non-perturbatively from phase-space considerations. Hence, the initial misalignment is bound to live in the $(-\pi, \pi]$ domain [26, 32].

[7] This implementation exploits the spectetor field approximation, by requiring the axion background energy budget to be negligible with respect to the total energy of the Universe.

JCAP06(2026)015

birefringence from CMB polarization [74, 75]. In particular, focusing on the EB cross-correlation only allows to avoid the cosmic variance associated with the temperature field and rises as a promising tool, given the higher predicted signal-to-noise ratio with respect to e.g. TB. Following the EB-estimator implemented by [66], we are able to reconstruct the harmonic coefficients associated with anisotropic birefringence from *Planck* NPIPE data. The related `HEALPix` [85] map at $N_{\rm side} = 64$ is shown in the left panel of figure 2. The latter is masked according to *Planck* NPIPE fiducial, with a corresponding sky fraction $f_{\rm sky} = 78\%$ (see right panel of figure 2). In addition, this dataset provides 400 simulations of polarization + noise that we use to obtain realizations of the anisotropic birefringence sky for covariance estimation, as discussed in section 4.2.

The birefringence maps used are generated with a minimum CMB multipole $\ell_{\rm min}^{\rm CMB} = 2$, in order to account for the polarization generated at all redshifts, particularly from both the recombination and reionization epochs. Ref. [66] demonstrates that the choice of $\ell_{\rm min}^{\rm CMB}$ has negligible impact on the birefringence auto-correlation, and we have tested that the same is true for the underlying cross-correlation. In this study, we aim to perform a 'blind' analysis to extract information on axion parameters from the complete birefringence signal, without isolating contributions from different cosmic epochs. Thus, the estimator from ref. [66] remains unaltered, though a different approach would be needed if our goal were to analyze birefringence at a specific redshift, as suggested by [86]. Given the extensive axion parameter space and the variability in dominant redshifts within it (see [54]), we avoid assumptions on the expected signal and proceed with an analysis on maps incorporating all birefringence contributions.

3.2 Quaia

Quasars offer as a powerful tool to probe accretion physics [87, 88], galaxy formation [89], supermassive black holes [90] and black hole evolution [91], gravitational lensing [92], halo masses [93] and the intergalactic medium [94]. Furthermore, quasars are exceptional tracers of large-scale-structure cosmology due to their position within peaks of the dark matter distribution, and can be exploited to constrain cosmological parameters [71, 95–103]. We consider the *Gaia-unWISE* Quasar catalog (Quaia), which is an all-sky sample comprising almost 1.3 million objects with magnitude $G < 20.5$, up to redshift $z \sim 3$. The catalog stems from the combination of quasar candidates in the third data release of *Gaia* [73] and the *unWISE* [104, 105] infrared photometry, based on the Wide-field Infrared Survey Explorer (*WISE*) [106]. The corresponding `HEALPix` distribution of sources,[8] at $N_{\rm side} = 64$, is illustrated in the top left panel of figure 3. Following refs. [70–72] we obtain the projected galaxy-overdensity in each pixel $\hat{\mathbf{n}}$ as $\delta_g(\hat{\mathbf{n}}) = N(\hat{\mathbf{n}})/(\bar{N}\omega(\hat{\mathbf{n}})) - 1$, where $N(\hat{\mathbf{n}})$ is the number of quasars in the pixel and $\omega(\hat{\mathbf{n}})$ the related selection function (shown in the top right panel of figure 3). Finally, $\bar{N} = \sum_{\hat{\mathbf{n}}} N(\hat{\mathbf{n}}) / \sum_{\hat{\mathbf{n}}} \omega(\hat{\mathbf{n}})$ is the mean number of sources per pixel. The resulting galaxy-overdensity map is depicted in the bottom left panel of figure 3. We mask all pixels in the sky where the selection function is lower than 0.5 (see bottom right panel of figure 3). To match the 400 birefringence simulated maps for covariance estimation, we

[8] The Quaia related data products have been produced following ref. [70] and are publicly available at https://zenodo.org/records/8060755.

JCAP06(2026)015

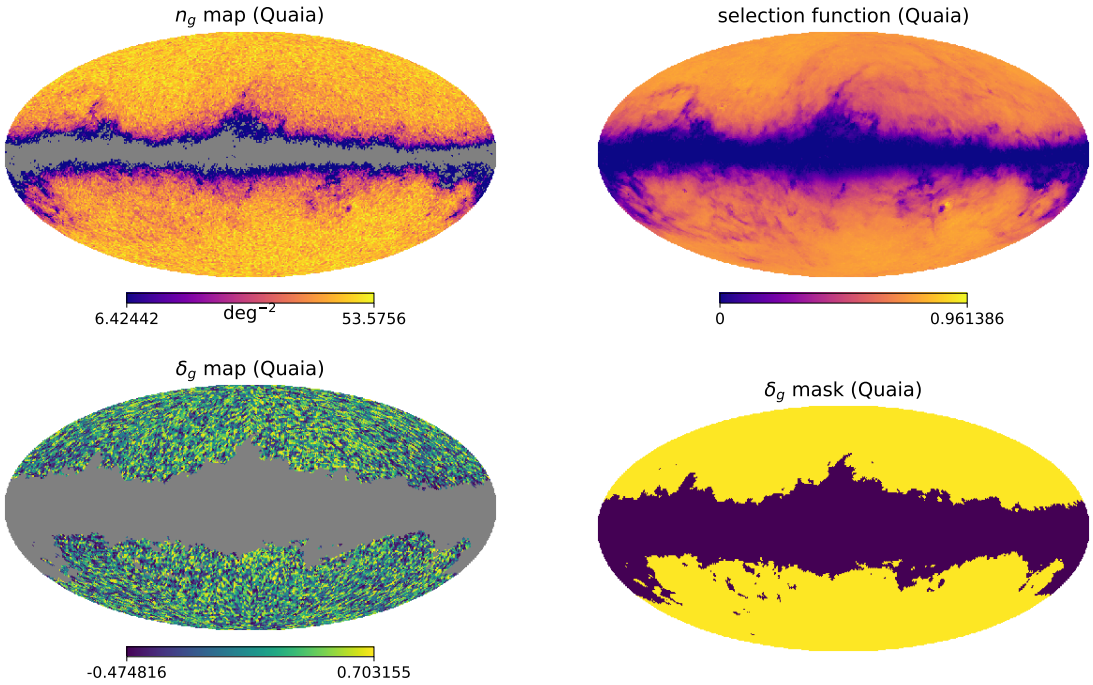


Figure 3. (*Top left*): pixel density of sources from the Quaia quasar catalog [70]; the map includes almost 1.3 million objects. (*Top right*): related selection function. (*Bottom left*): galaxy overdensity from Quaia derived as outlined in section 3.2. (*Bottom right*): Quaia sky mask. Reproduced from [70]. CC BY 4.0.

generate an equal number of realizations of δ_g by reshuffling a random catalog with ten times the sources of the data catalog outlined above.[9]

4 Methodology

We review here the theoretical formulation of the birefringence-galaxy cross-correlation, first proposed in [54], with particular attention to key ingredients related to the chosen data (see section 3). We then summarize the strategy adopted to extract the observed underlying cross-correlation.

4.1 Power spectrum estimation

We derive the observed cross-correlation angular power spectrum from the data of section 3 through a *pseudo-*C_ℓ estimator [107] at $\ell > 12$, whilst exploiting a quadratic maximum likelihood (QML) approach for the first multipoles.[10]

***Pseudo-*C_ℓ.** This estimator works in harmonic space and, taking advantage of its extremely fast computation times, is particularly suited for large datasets. Nonetheless, dealing with

[9] Each galaxy realization conserves the total number of sources of the data-map.

[10] During the process, we take into account deprojection effects by applying a systematic-template for Quaia quasars to the estimates, following ref. [70]. We find negligible variations, as also deeply studied in [108]. Furthermore, we minimize dipole leakage on the derived spectra by adding a constant template to the covariance.

JCAP06(2026)015

spherical harmonic transforms of masked data introduces information loss and mode mixing, especially at the largest scales. Following the `NaMaster` [109] implementation, the pseudo angular power spectrum is

$$\tilde{C}_\ell^{\alpha g} = \frac{1}{2\ell+1} \sum_{m=-\ell}^{+\ell} \tilde{a}_{\ell m}^{\alpha}\, \tilde{a}_{\ell m}^{g*}\,, \tag{4.1}$$

where the harmonic coefficients for a generic field $X(\hat{\mathbf{n}})$ come from its expansion on spherical harmonics over a masked region of the sky, defined by the weight function $w_{\hat{\mathbf{n}}}^X$,

$$\tilde{a}_{\ell m}^X = \int \mathrm{d}\Omega\; X(\hat{\mathbf{n}})\, w_{\hat{\mathbf{n}}}^X\, Y_{\ell m}^*(\hat{\mathbf{n}})\,. \tag{4.2}$$

The unbiased estimator of the true power spectrum for our cross-correlation[11] is then:

$$\hat{C}_\ell^{\alpha g} = \sum_{\ell'} M_{\ell\ell'}^{-1} \tilde{C}_{\ell'}^{\alpha g}\,, \tag{4.3}$$

with $M_{\ell\ell'}^{-1}$ accounting for the incomplete sky coverage

$$\begin{aligned} M_{\ell\ell'}^{\alpha g} &= \frac{(2\ell'+1)}{4\pi} \sum_{\ell''} (2\ell''+1)\, \tilde{W}_{\ell''}^{\alpha g} \begin{pmatrix} \ell & \ell' & \ell'' \\ 0 & 0 & 0 \end{pmatrix}^2, \\ \tilde{W}_\ell^{\alpha g} &= \frac{1}{2\ell+1} \sum_{m=-\ell}^{\ell} \tilde{w}_{\ell m}^{\alpha}\, \tilde{w}_{\ell m}^{g*}\,. \end{aligned} \tag{4.4}$$

Here, the last term in the first line is a Wigner 3-j symbol [110], whilst $w_{\ell m}^{\alpha}$ and $w_{\ell m}^{g}$ are the spherical harmonic coefficients of the two probes' masks, respectively. Due to the relatively strong bias, at large scales, brought in by eq. (4.4), we trust only estimates for $\ell > 12$, up to $\ell_{\rm max} = 3N_{\rm side} - 1$.

QML. This estimator [111, 112], on the contrary, works in pixel space, sensibly reducing masking effects at low multipoles. However, dealing with several pixel-pixel matrices is computationally demanding. The underlying algebra yields

$$\hat{C}_\ell^{\alpha g} = F_{\ell\ell'}^{-1}\, y_{\ell'}\,, \tag{4.5}$$

where the Fisher matrix $F_{\ell\ell'}$ and the minimum-variance quadratic estimator y_ℓ are defined as follows:

$$\begin{aligned} F_{\ell\ell'} &= \mathrm{Tr}\left[\mathtt{C}_{\alpha\alpha}^{-1}\, \mathtt{P}_\ell \mathbf{C}_{gg}^{-1}\, \mathtt{P}_{\ell'}^T\right], \\ y_\ell &= \boldsymbol{\alpha}^T \mathtt{C}_{\alpha\alpha}^{-1}\, \mathtt{P}_\ell \mathtt{C}_{gg}^{-1} \boldsymbol{\delta_g}\,. \end{aligned} \tag{4.6}$$

$\mathtt{C}_{\alpha\alpha}$ and $\mathtt{C}_{gg}$ are the signal covariance matrices, related to the two data vectors in pixel space $\boldsymbol{\alpha}$ and $\boldsymbol{\delta_g}$. The matrix elements of $\mathtt{P}_\ell$ are $\mathrm{P}_{\ell,ij} = (2\ell+1)/4\pi\; p_\ell(\hat{\mathbf{n}}_i \cdot \hat{\mathbf{n}}_j)$, defined through the Legendre polynomials $p_\ell(\hat{\mathbf{n}}_i \cdot \hat{\mathbf{n}}_j)$. Eq. (4.5) is an unbiased estimator of the underlying cross-correlation ($\langle \hat{C}_\ell^{\alpha g} \rangle = C_\ell^{\alpha g}$), and we utilize it to derive the power spectrum at $\ell \leq 12$.

[11] Let us notice how eq. (4.3) does not include a noise power spectrum, as the latter only appears for auto-correlations.

JCAP06(2026)015

4.2 Covariance estimation

We estimate the covariance matrix of the cross-correlation as

$$\hat{\mathsf{C}}^{\alpha g}_{\ell\ell'} = \frac{1}{n-1}\sum_{k=1}^{n}\left(\hat{C}^{\alpha g(k)}_{\ell} - \langle\hat{C}^{\alpha g(k)}_{\ell}\rangle\right)\left(\hat{C}^{\alpha g(k)}_{\ell'} - \langle\hat{C}^{\alpha g(k)}_{\ell'}\rangle\right), \tag{4.7}$$

with $n = 400$ realizations of anisotropic birefringence and galaxy overdensity outlined in section 3. It can be demonstrated that this provides an unbiased estimate of the true covariance matrix $\boldsymbol{\Sigma}$ as long as $p < n - 1$, with p being the length of the data vector $\hat{C}^{\alpha g}_{\ell}$. However, for our analysis, we require the inverse covariance matrix for both goodness-of-fit assessments and parameter estimation (see section 5). As shown in ref. [113], $(\hat{\mathsf{C}}^{\alpha g}_{\ell\ell'})^{-1}$ is a biased estimator of the true inverse covariance $\boldsymbol{\Sigma}^{-1}$ due to noise injected in $\hat{\mathsf{C}}^{\alpha g}_{\ell\ell'}$ as p approaches n. To first order, this issue can be mitigated by either re-normalizing the estimated inverse covariance [113] or marginalizing over the true covariance matrix, conditioned on its estimate [114]. Furthermore, binning the data vector helps to reduce the noise in the off-diagonal elements of the estimated covariance by compensating for the limited number of realizations. Ideally, the data vector length should be reduced to $\tilde{p}$, the maximum size that still allows for reliable covariance estimation given the number of simulations n, satisfying $\tilde{p}(\tilde{p}+1)/2 < n$. For 400 realizations, this yields $\tilde{p} \sim 27$. In what follows, we will adopt the least aggressive binning scheme possible and further examine the impact of binning in appendix A.

Additionally, the random catalog utilized to extract the 400 realizations of galaxy overdensity lacks the large-scale systematics present in the associated data. To address this, we calibrate the effective degrees of freedom, $\nu_{\rm eff}$, from the aforementioned realizations and subsequently re-normalize the covariance of eq. (4.7) by the variance analytically derived from the data with the calibrated $\nu_{\rm eff}$. This process can be summarized as follows

$$\begin{aligned}
\hat{\mathsf{C}}^{\alpha g}_{\rm new} &= \hat{\mathsf{C}}^{\alpha g}\frac{\sigma_{\rm dat,\,eff}\otimes\sigma_{\rm dat,\,eff}}{\sigma_{\rm sim}\otimes\sigma_{\rm sim}}\,,\\
\sigma_{\rm sim} &= \sqrt{{\rm diag}(\hat{\mathsf{C}}^{\alpha g})}\,,\\
\sigma_{\rm dat,\,eff} &= \sqrt{\frac{1}{\nu_{\rm eff}}\left((\hat{C}^{\alpha g}_{\ell,\,\rm dat})^2 + \hat{C}^{\alpha\alpha}_{\ell,\,\rm dat}\hat{C}^{gg}_{\ell,\,\rm dat}\right)}\,,\\
\nu_{\rm eff} &= \frac{(\hat{C}^{\alpha g}_{\ell,\,\rm sim})^2 + \hat{C}^{\alpha\alpha}_{\ell,\,\rm sim}\hat{C}^{gg}_{\ell,\,\rm sim}}{\sigma^2_{\rm sim}}\,,
\end{aligned} \tag{4.8}$$

where $\sigma_{\rm sim}$ represents the standard deviation derived from eq. (4.7) exploiting the 400 realizations of the underlying spectra, with their means denoted as $\hat{C}^{\alpha g}_{\ell,\,\rm sim}$, $\hat{C}^{\alpha\alpha}_{\ell,\,\rm sim}$ and $\hat{C}^{gg}_{\ell,\,\rm sim}$. Meanwhile, $\sigma_{\rm dat,\,eff}$ refers to the analytical standard deviation calculated from the data ($\hat{C}^{\alpha g}_{\ell,\,\rm dat}$, $\hat{C}^{\alpha\alpha}_{\ell,\,\rm dat}$ and $\hat{C}^{gg}_{\ell,\,\rm dat}$), adjusted using the effective degrees of freedom $\nu_{\rm eff}$. The $\otimes$ product refers to the outer product to compute the correlation matrix ρ related to both simulations and data ($\rho = \sigma \otimes \sigma$). The covariance structure is illustrated in figure 4, where we present $\hat{\mathsf{C}}^{\alpha g}_{\rm new}/\sqrt{{\rm diag}(\hat{\mathsf{C}}^{\alpha g}_{\rm new})}\otimes\sqrt{{\rm diag}(\hat{\mathsf{C}}^{\alpha g}_{\rm new})}$, excluding the diagonal elements, for four different binning schemes ($\Delta\ell = 1$, $\Delta\ell = 5$, $\Delta\ell = 10$, $\Delta\ell = 19$). This representation is valuable for analyzing the off-diagonal contributions and shows how binning reduces correlations coming from the off-diagonal structure. For the least aggressive cases, the initial off-diagonal terms exhibit mild anti-correlation.

JCAP06(2026)015

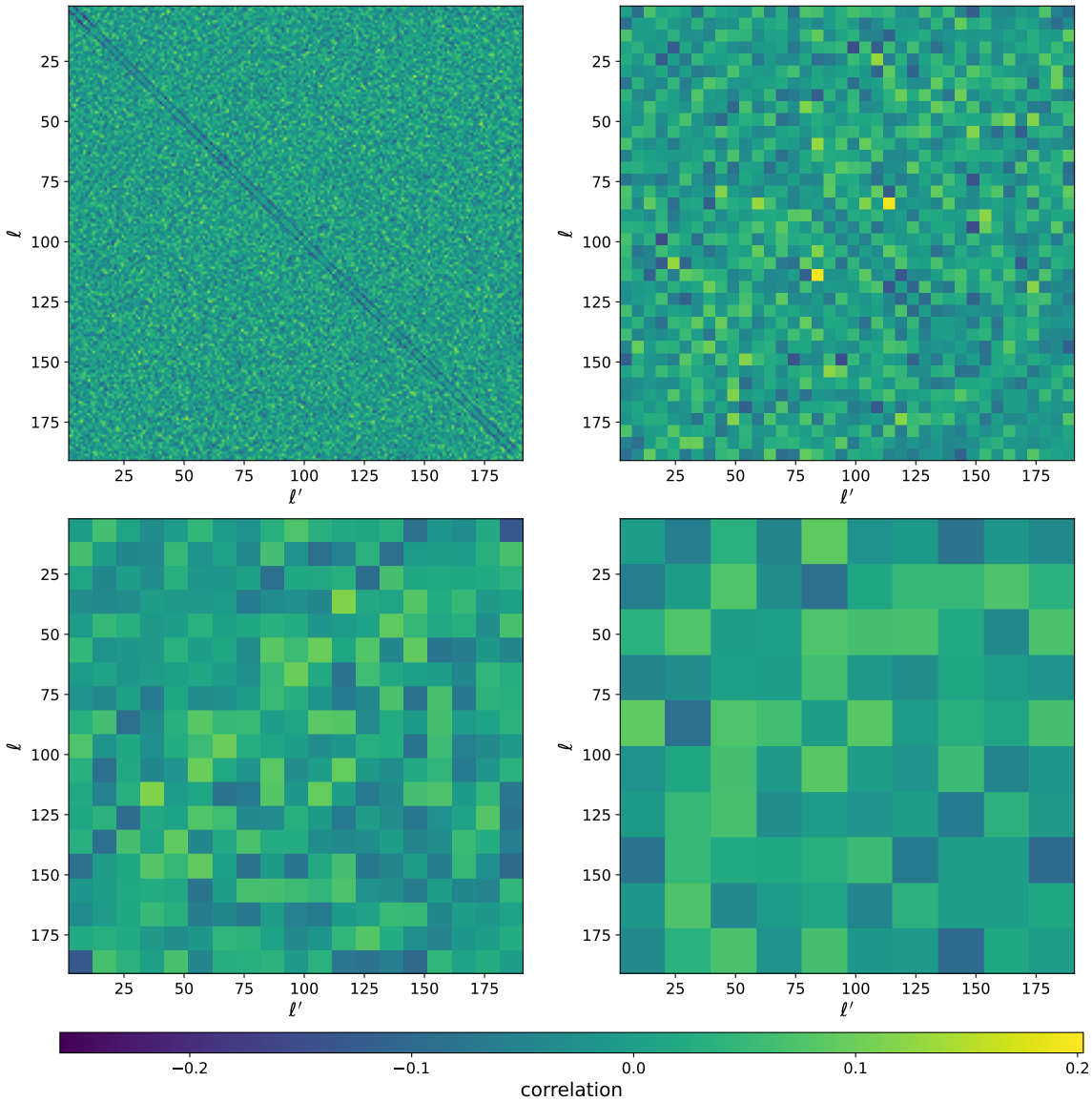


Figure 4. Correlation matrix obtained from the covariance of eq. (4.8) with the diagonal subtracted. We exploit a QML estimator for the first 12 multipoles, and *pseudo-*C_ℓ's afterwards (see section 4.1). (*Top left*): no binning, $\Delta\ell = 1$. (*Top right*): 5 multipoles per bandpower, $\Delta\ell = 5$ (38 bins). (*Bottom left*): 10 multipoles per bandpower, $\Delta\ell = 10$ (19 bins). (*Bottom right*): 19 multipoles per bandpower, $\Delta\ell = 19$ (10 bins).

5 Results

The focus of this paper is to present, for the first time, a measurement of the cross-correlation between anisotropic birefringence and galaxies. Both probes stem from the metric perturbations and a detection of such a signal would not only raise valuable insights about cosmic birefringence, but also allow constraining the underlying axion-parameters [54]. Exploiting a combined QML/*pseudo-*C_ℓ analysis, we derive the observed angular power spectrum from *Planck* NPIPE polarization data and Quaia galaxy overdensity. We show how this signal is

JCAP06(2026)015

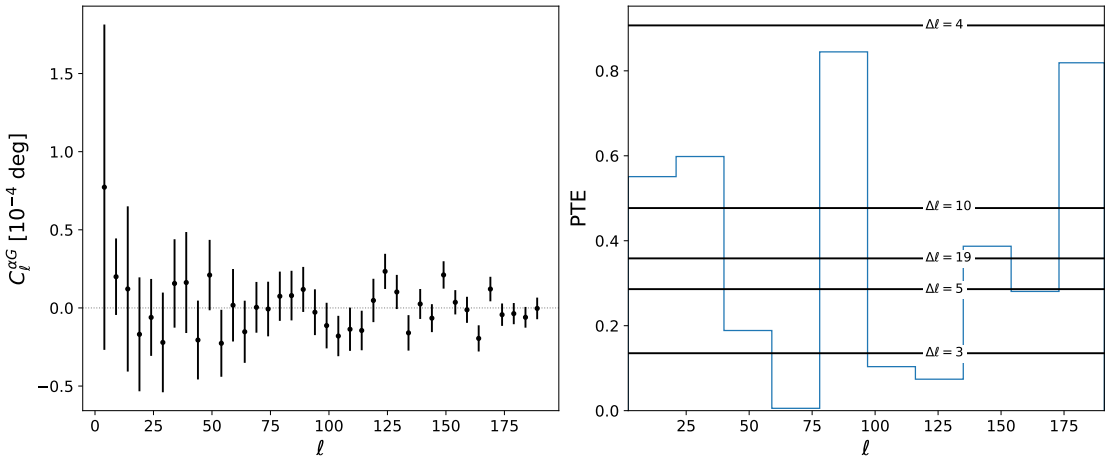


Figure 5. (*Left*): cross-correlation angular power spectrum between anisotropic birefringence and galaxy number counts, as measured by the combination of *Planck* NPIPE polarization data and the quasar catalog Quaia. The signal is binned with $\Delta\ell = 5$ bandwidth and error bars are computed from the covariance estimated with 400 realizations of the two probes (see section 4.2). (*Right*): the black horizontal lines corresponds to the PTE obtained across the entire range of multipoles with different binning schemes as indicated by the related bandwidth $\Delta\ell$. The blue line represents the PTE achievable within a specific chunk of multipoles and $\Delta\ell = 1$.

well compatible with the null-hypothesis and compare it with the theoretical power spectrum to impose a novel bound on the axion-photon coupling for ultralight axions.

5.1 The measured cross-correlation

As discussed in section 4, we estimate the underlying cross-correlation angular power spectrum utilizing a QML estimator for $\ell = [2, 12]$ and a *pseudo-*C_ℓ estimator for $\ell = [13, 191]$.[12] The maximum multipole of our analysis stems from the resolution of the datasets under consideration ($\ell_{\rm max} = 3N_{\rm side} - 1$ with $N_{\rm side} = 64$). The estimators are applied to the maps and related masks, presented in section 3. Anisotropic birefringence is associated with the *Planck* NPIPE polarization dataset, whilst the spatial distribution of galaxies is derived from the Quaia quasar catalog.

The result is shown in the left panel of figure 5 with 5-multipoles per bandpower. The associated error bars spring from the diagonal of the covariance in eq. (4.8). This signal is compatible with the null-hypothesis with a probability to exceed (PTE) of 29%. The compatibility is retained across different binning strategies and shown in the right panel of figure 5 for $\Delta\ell = 3$, 4, 5, 10 and 19. Only the unbinned and $\Delta\ell = 2$ spectrum yield poor compatibility with the null-hypothesis (PTE $\ll 5\%$) due to the high level of correlation in the off-diagonal structure of the covariance (see figure 4). Let us highlight that the following results show little to no change when varying the binning scheme (for further details on the impact of binning refer to appendix A). The right panel of figure 5 also illustrates how the

[12] Let us remind that this choice is due the inefficiency of *pseudo-*C_ℓ's to correctly estimate power spectra at large scales, where masking effects in harmonic space are dominant.

JCAP06(2026)015

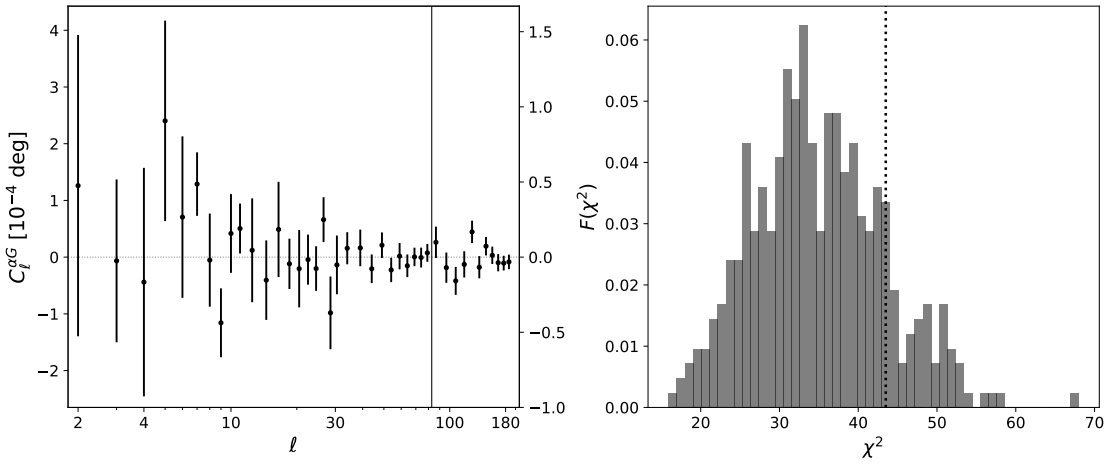


Figure 6. (*Left*): Planck NPIPE cross Quaia angular power spectrum between anisotropic birefringence and galaxy number counts. We use the following binning scheme: no binning for the first 10 multipoles, 10 bins with 2 multipoles, 10 bin with 5 multipoles and 10 multiples per bandpower afterwards. The result is divided in two y-scale regions for visualization purposes. (*Right*): corresponding Gaussian chi-squared distribution from the 400 realizations. The dotted vertical line refers to the data χ^2 of the left panel.

measured cross-correlation stems compatibility with the null-hypothesis in selected chunks of multipoles.[13] Each of the ten chunks contains 19 multipoles, with a $\Delta\ell = 1$ bandwidth.

For parameter estimation, in section 5.3, we will utilize the following binning scheme: $\Delta\ell = 1$ for the first 10 multipoles, $\Delta\ell = 2$ for the following 20 multipoles, $\Delta\ell = 5$ for the consequent 50 multipoles and $\Delta\ell = 10$ for the rest. This approach minimizes information loss on large scales, where our theoretical analysis predicts the greatest power [54]. This binning strategy remains compatible with zero, with a PTE of 37%. The left panel of figure 6 shows its angular power spectrum, while the right panel illustrates the corresponding Gaussian null-hypothesis χ^2 for data, overlapped with the distribution given by the 400 realizations used to estimate the covariance matrix.

We emphasize how this is the first measurement of such a correlation and future CMB polarization experiments [115–117], together with forthcoming galaxy surveys [118–121], could enhance the signal-to-noise ratio and eventually reveal an excess of power (see e.g. [54]). In figure 7 we compare the measured cross-correlation with theoretical predictions for a set of given ALPs parameters.

5.2 Scale invariant amplitude

As an extra test of data compatibility with the null-hypothesis, we perform a Gaussian likelihood on the scale-invariant amplitude, A, of the α-G cross-correlation field:

$$-2\log\mathcal{L}(A) = (C_\ell - A)\,(\mathsf{C}^{-1})_{\ell\ell'}\,(C_{\ell'} - A)^T\,, \tag{5.1}$$

where the superscript αg is implied and $(\mathsf{C}^{-1})_{\ell\ell'}$ is the inverse covariance matrix derived from eq. (4.8). From eq. (5.1) we derive the best fit value of the amplitude and the related

[13] Only the chunk around $\ell = 60$ results in a low PTE due to the off-diagonal terms of the covariance being the strongest in this region (see figure 4).

JCAP06(2026)015

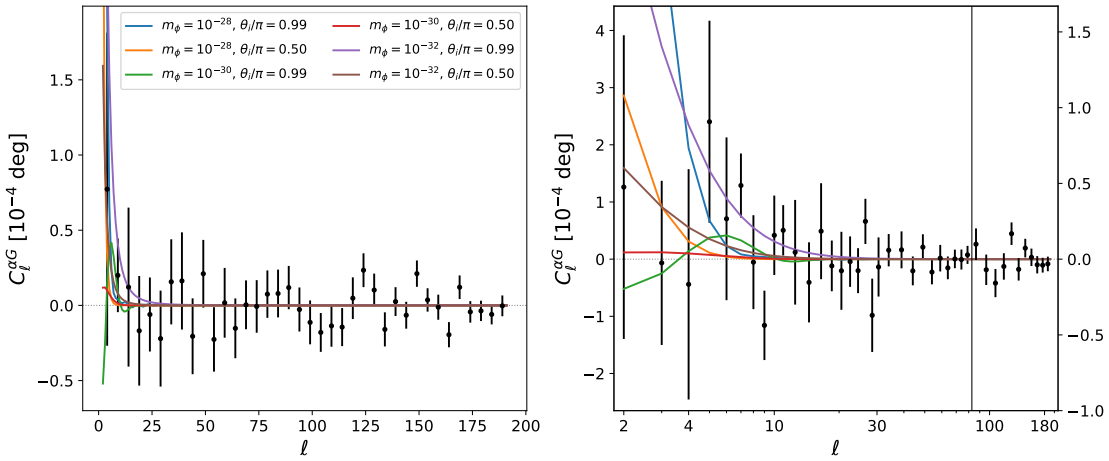


Figure 7. Measured cross-correlation and theoretical predictions for a set of given ALPs parameters ($g_{\phi\gamma} = 2 \times 10^{-14}\,\mathrm{GeV}^{-1}$). The mass m_ϕ is reported in eV.

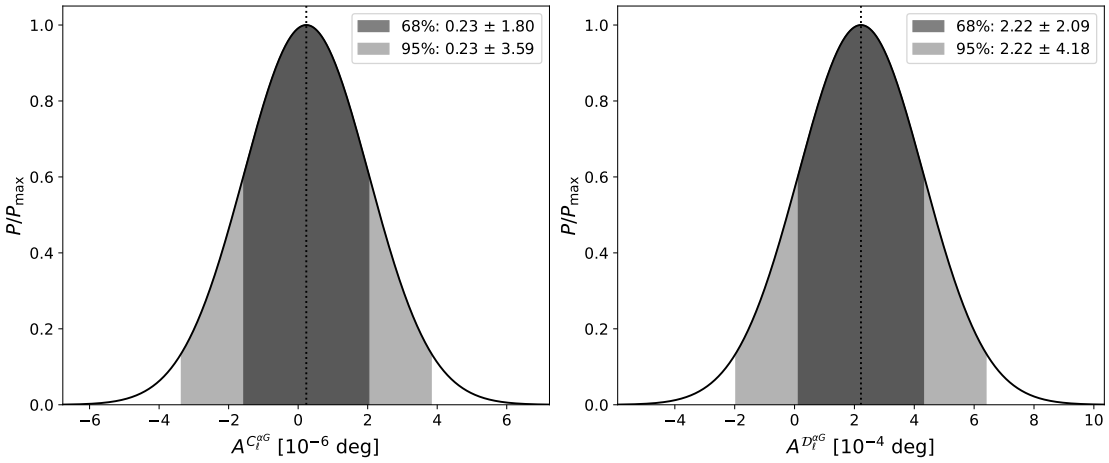


Figure 8. Posterior on a scale invariant amplitude A, fitted on the observed spectrum of figure 5 with a Gaussian likelihood, both for C_ℓ's (*Left*) and $\mathcal{D}_\ell$'s (*Right*). The dark(light) shaded region corresponds to the 68(95)% confidence level.

68% and (95%) confidence interval (we use a 5-multipole per bandpower binning scheme): $A^{C_\ell} = [0.23 \pm 1.80(3.59)] \times 10^{-6}$ deg. We also fit a constant amplitude on $\mathcal{D}_\ell = \ell(\ell+1)/2\pi\, C_\ell$, by replacing it to C_ℓ both for the data vector and the covariance of eq. (5.1). We obtain $A^{\mathcal{D}_\ell} = [2.22 \pm 2.09(4.18)] \times 10^{-4}$ deg. The two results are depicted in figure 8. Additionally, we calculated both values using an unbiased inverse covariance following Hartlap et al. [113], and by adjusting the likelihood in eq. (5.1) according to the method in ref. [114], which marginalizes over the true covariance matrix. As discussed in section 4.2, these approaches account for the limited number of realizations and broaden the posterior distribution. Consequently, the resulting confidence levels are increased by approximately 3% (the effect would be greater for less aggressive binning schemes).

JCAP06(2026)015

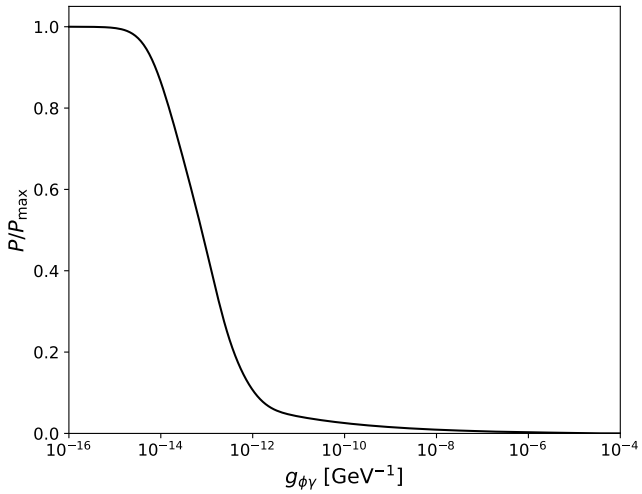


Figure 9. Posterior distribution on the axion-photon coupling $g_{\phi\gamma}$ marginalized on the other two free parameters (mass and initial misalignment). As the coupling increases, the predicted spectrum from eq. (2.1) becomes larger, eventually deviating from observations and thus resulting in a lower probability.

5.3 Bound on axion-photon coupling

In section 2 we have reviewed the theoretical formulation of the birefringence-galaxy cross-correlation and its implementation in our modified version of `CLASS`. In particular, we have discussed how the latter depends on the axion mass m_ϕ, the initial misalignment θ_i and the axion-photon coupling $g_{\phi\gamma}$. As extensively outlined in refs. [45, 48, 54], ultralight axions with $m_\phi < 10^{-28}\,\mathrm{eV}$ offer as a promising tool to constrain birefringence and can provide a suitable explanation [48] for the latest measurements of the isotropic CB angle [61, 122]. While the mass and the misalignment mainly govern the shape of the predicted cross-correlation signal, due to their non trivial behavior within eq. (2.1), the axion-photon coupling controls directly the amplitude, appearing as a multiplicative factor. We anticipate a probability close to unity for all "small enough" couplings, given the measured power spectrum's compatibility with the null-hypothesis, whilst as the coupling increases the theoretical model will exceed observations and eventually an upper bound on $g_{\phi\gamma}$ can be imposed. Previous works have constrained this coupling through haloscopes, helioscopes, colliders, and astrophysical searches (for comprehensive data and references, refer to `AxionLimits` [123]). These constraints extend down to $m_\phi \sim 10^{-12}\,\mathrm{eV}$, with extensions to $10^{-24}\,\mathrm{eV}$ from isotropic birefringence [124, 125] and black hole polarimetry [126]. Ref. [48] probes a combination of axion parameters in the mass range $m_\phi \in (10^{-33},\, 10^{-26})$ eV, making use of the isotropic birefringence angle from ref. [60]. Our analysis targets an ultra-low mass regime, where, to date, no direct constraint on the axion-photon coupling has been reported in the literature.

We explore the axion-parameter space with a Gaussian likelihood

$$-2\log\mathcal{L}(\Theta) = (C_\ell^{\mathrm{th}}(\Theta) - C_\ell^{\mathrm{obs}})\,(\mathsf{C}^{-1})_{\ell\ell'}\,(C_\ell^{\mathrm{th}}(\Theta) - C_\ell^{\mathrm{obs}})^T\,, \tag{5.2}$$

where C_ℓ^{th} is the predicted power spectrum from the theoretical model of eq. (2.1) with parameters $\Theta = (m_\phi,\, \theta_i,\, g_{\phi\gamma})$, C_ℓ^{obs} the observed power spectrum as discussed in sec-

JCAP06(2026)015

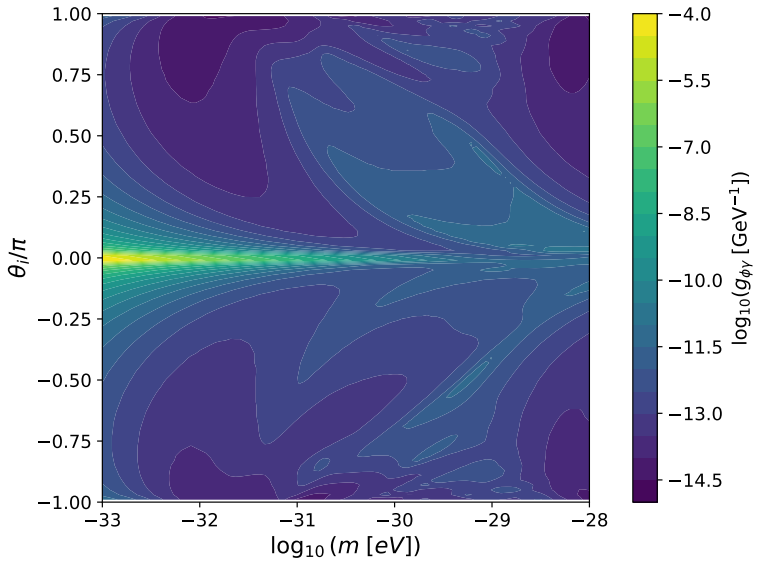


Figure 10. Achievable upper bound on the axion-photon coupling, at the 95% confidence level, for each point in the m_ϕ-θ_i parameter space. For very small misalignment angles, the theoretical power spectrum is significantly reduced, requiring a higher value of $g_{\phi\gamma}$ to enhance the signal sufficiently away of observations.

tion 5.1, and $(\mathsf{C}^{-1})_{\ell\ell'}$ the inverse of the covariance matrix of eq. (4.8). We consider $m_\phi \in [10^{-33}, 10^{-28}]$ eV,[14] and $\theta_i \in (-\pi, \pi)$, whereas we let the coupling vary, in principle, between 0 and ∞.

The marginalized posterior distribution on $g_{\phi\gamma}$ is shown in figure 9. The region of highest probability contains couplings smaller than $\sim 10^{-12}\,\mathrm{GeV}^{-1}$, but a significant portion of the probability density extends to the tail of the distribution. At the 95% confidence level, the upper bound reaches over $10^{-5}\,\mathrm{GeV}^{-1}$. This is primarily due to a degeneracy with the initial misalignment, which also determines the starting value of the axion field. Consequently, when $|\theta_i| \sim 0$, the cross-correlation is null regardless of the coupling value. To address this, we derive an upper bound for each point in the m_ϕ-θ_i parameter space, presenting our results in figure 10. The regions with the strongest upper bounds are those where $m_\phi \sim 10^{-32}\,\mathrm{eV}$ and the misalignment angle is high. This result aligns with our previous theoretical analysis [54]. In figure 11, we also show the corresponding curves in the coupling-mass plane at fixed values of θ_i. It is clear that the closer the initial misalignment is to zero, the less stringent the obtained bound becomes. In conclusion, cross-correlating anisotropic birefringence with galaxies using the currently available data allows us to set an upper bound on the axion-photon coupling down to $\sim 10^{-15}\,\mathrm{GeV}^{-1}$ in the most favorable region of our parameter space. This makes for an unprecedented result in the ultralight axion mass range under

[14] The lowest mass roughly corresponds to the Hubble parameter today and even lower masses would lead to fields whose dynamical evolution has not commenced yet. We do not explore the region where $m_\phi > 10^{-28}\,\mathrm{eV}$ as it is computationally demanding and the perturbative approach breaks [54].

JCAP06(2026)015

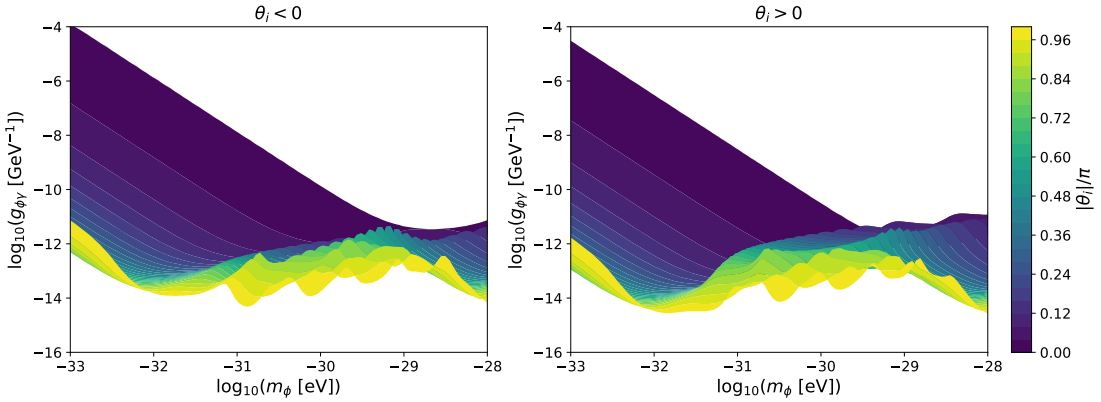


Figure 11. Upper bound, at 95% confidence level, on the axion-photon coupling as a function of the axion mass. Each line is drawn for a fixed value of the initial misalignment angle, depicted in the colorbar. It is evident how the tightest constraints are obtained for high values of the latter, where there is no degeneracy with the coupling.

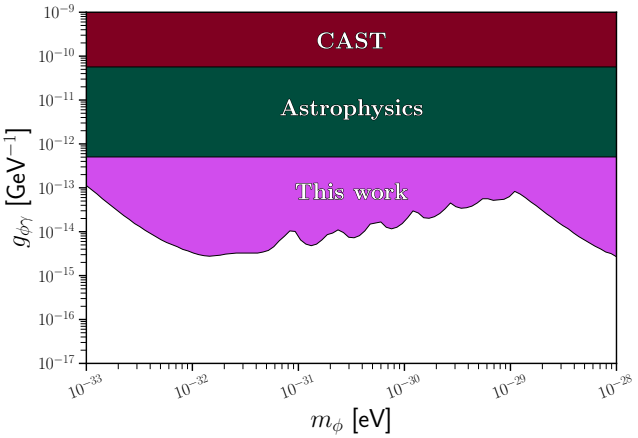


Figure 12. Best achievable upper bound, at 95% confidence level, on the axion-photon coupling, $g_{\phi\gamma}$, as a function of the axion mass, m_ϕ, as derived from the cross-correlation analysis of *Planck* PR4 birefringence and Quaia galaxy number counts considering for each mass the value of $|\theta_i|/\pi$ which provides the most stringent constraint. This is equivalent of taking the lowermost curve in figure 11. We compare the result with the extension to lower masses of current bounds, derived in a higher mass range. [123].

consideration, significantly improving upon existing astrophysical and laboratory bounds at higher masses[15] (see figure 12).

6 Conclusion

In this study, we have presented, for the first time, the measurement of the cross-correlation between anisotropic cosmic birefringence and the spatial distribution of galaxies. The rotation of the linear polarization plane of the CMB can be caused by axion-like components coupling to photons with parity-violating terms. The evolution of these pseudo-scalars is governed by

[15]These upper bounds are formally valid for $m_\phi > 10^{-24}$ eV and have been linearly extrapolated into our mass range solely for comparison purposes.

JCAP06(2026)015

the interplay between their potential and metric perturbations, the latter being responsible for the collapse of structures into forming galaxies. This cross-correlation signal is not only expected to be non-zero but also serves as a valuable probe of the underlying axion model.

We computed the observed power spectrum by combining *Planck* NPIPE polarization data with the Quaia quasar catalog. By applying an EB-estimator on the former, we obtained a birefringence map across the sky at $N_{\rm side} = 64$. Similarly, we calculated the corresponding galaxy overdensity map using the 1.3 million sources from the latest Quaia release. We applied a QML estimator at $\ell < 12$, integrated with a *pseudo-*C_ℓ estimator at larger multipoles. We computed the related covariance matrix from 400 realizations of the two probes and showed that our measurement is well compatible with zero, with a PTE between 20% and 80% depending on the binning scheme. This compatibility is also retained across selected chunks of the entire multipole range.

With the aim of setting an unprecedented upper bound on the axion-photon coupling for ultralight candidates with masses in the range $(10^{-33}, 10^{-28})$ eV, we performed a Gaussian likelihood analysis on the following free parameters: the mass m_ϕ, the initial misalignment angle θ_i, and the axion-photon coupling $g_{\phi\gamma}$. Due to a degeneracy of the coupling with the very small end of the initial misalignment, we were unable to retrieve a competitive upper bound with the full normalization of the other two parameters. Nonetheless, we explored the attainable bound at each point in the mass-misalignment parameter space and found values down to $10^{-15}\,\mathrm{GeV}^{-1}$. Specifically, our findings reach 95% upper limits of up to 10^{-14} GeV^{-1} on the axion-photon coupling, for the misalignment angle condition $|\theta_i|/\pi \geq 0.7$ or 10^{-13} GeV^{-1} for $|\theta_i|/\pi \geq 0.4$. For masses around 10^{-32} eV and high initial misalignment angles, i.e. $|\theta_i|/\pi \geq 0.99$, we obtain an unprecedented upper bound on the axion-photon coupling down to $g_{\phi\gamma} = 10^{-15}$ GeV^{-1}.

In light of the incoming data from next-generation galaxy surveys and CMB polarization experiments, the novelty of this probe lies in its capability to effectively constrain the axion-parameter in a poorly bounded mass range. Additionally, a detection of such a signal could significantly contribute to the open question of the existence of cosmic birefringence and the underlying parity-violating physics.

Acknowledgments

We thank M. Ballardini, L. Caloni and G. Galloni for valuable discussions. We also convey our appreciation towards the Institute for Fundamental Physics of the Universe (IFPU), that hosted the focus week "Parity violation through CMB observations",[16] where the many insights enabled us to get this work started. We acknowledge financial support from the INFN InDark initiative and from the COSMOS network (www.cosmosnet.it) through the ASI (Italian Space Agency) Grants 2016-24-H.0, 2016-24-H.1-2018 and 2020-9-HH.0. We acknowledge the use of CINECA HPC resources from the InDark project in the framework of the INFN-CINECA agreement. SA and ML acknowledge participation in the COST Action CA21106 "COSMIC WISPers", supported by COST (European Cooperation in Science and Technology). SA and GZ acknowledge financial support by "Bando Giovani anno 2023 per progetti di ricerca

[16] https://www.ifpu.it/focus-week-2024-05-27/.

JCAP06(2026)015

finanziati con il contributo 5x1000 anno 2021". NB, AG and PN acknowledges support by the MUR PRIN2022 Project "BROWSEPOL: Beyond standaRd mOdel With coSmic microwavE background POLarization"-2022EJNZ53 financed by the European Union — Next Generation EU. We express our gratitude to Led Zeppelin for inspiring us on the challenging journey towards uncovering dark components, our cosmological "heaven".

A Impact of binning and galaxy bias model

As discussed in section 4.2, the covariance matrix in eq. (4.7) may exhibit excessive noise in its off-diagonal elements due to the limited number of realizations used for estimation, potentially leading to bias in the inverse covariance matrix. Increasing the level of binning helps mitigate this bias by reducing strong or anomalous correlations in off-diagonal terms, though at the cost of some information loss, which may warrant alternative strategies. Hartlap et al. [113] provide a first-order correction for this bias through a constant (Hartlap) factor, dependent on the length of the data vector p and the number of simulations n used to estimate the covariance:

$$(\hat{\mathsf{C}}^{-1})^{\alpha g}_{\ell\ell'} = \frac{n-p-2}{n-1}(\hat{\mathsf{C}}^{\alpha g}_{\ell\ell'})^{-1} \quad \text{for } p < n-2\,. \tag{A.1}$$

In this context, the inverse matrix of eq. (4.7) tends to be increasingly overestimated as the length of the data vector approaches the number of available simulations. Notably, when $p \ll n$, the correction factor in eq. (A.1) is close to unity. In cosmology, this often results in an artificially heightened constraining power for parameter estimation. Applying the Hartlap correction factor addresses this by broadening posterior distributions and thereby increasing confidence intervals on parameter estimates. Sellentin and Heavens [114] suggest that this adjustment introduces heavy tails in the posterior, and propose a more precise method that involves marginalizing over the true covariance matrix, conditioned on its estimate, thus relaxing the Gaussian assumption in the likelihood. This approach effectively results in a t-distribution, where both mean and variance are treated as random variables. The modified likelihood thus becomes

$$-2\ln\mathcal{L} = n\ln\left(1+\frac{\chi^2}{n-1}\right), \tag{A.2}$$

where χ^2 is the standard Gaussian likelihood.

We evaluated the effects of using a binning scheme and applying each correction on our results. The cross-correlation signal shown in figure 5 remains consistent with zero regardless of the binning choice, and neither the Hartlap factor nor the modified likelihood affects goodness-of-fit tests.[17] The left panel of figure 13 shows the PTE of the null-hypothesis as a function of binning bandwidth, $\Delta\ell$. Only the unbinned and 2 multipoles per bin cases produce a value below 5%, due to significant off-diagonal correlations in the covariance matrix, which are mitigated with increased binning bandwidth. In figure 14, we also present the χ^2 distribution from 400 realizations, with the data value (marked as a vertical line) well within the distribution for all but the first two cases.

[17] This occurs because the data's χ^2 shifts along with the underlying distribution, resulting in an unchanged PTE.

JCAP06(2026)015

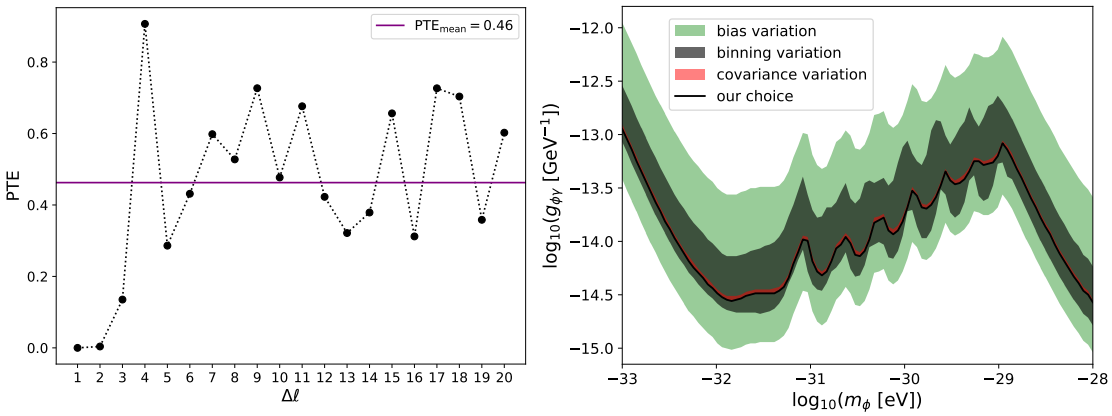


Figure 13. (*Left*): value of the PTE as a function of binning bandwidth $\Delta\ell$. Each value corresponds to the compatibility of the measured cross-correlation with zero. (*Right*): maximal variation of the axion-photon coupling, as a function of mass, upon variations of the bias (light green), the binning bandwidth (gray) or the covariance estimation and consequent likelihood choice (red), as described in the text. The black line refers to our baseline: no correction applied on the covariance, a mixed binning (10 bins with $\Delta\ell = 1$, 10 with $\Delta\ell = 2$, 10 with $\Delta\ell = 5$ and $\Delta\ell = 10$ afterwards) and $b_g = 1$ corresponding to the bias in eq. (2.6).

For parameter estimation, the achievable upper bound on the axion-photon coupling is modestly influenced by the choice of binning scheme. More aggressive binning results in less stringent bounds due to information loss on large scales, where the theoretical signal is expected to be strongest [54]. The maximum observed variation in the best $g_{\phi\gamma}$-m_ϕ bound of figure 11 reaches about half an order of magnitude. This variation diminishes to a few percent as the binning bandwidth exceeds $\Delta\ell \sim 5$, likely indicating that no further large-scale information is being lost. This outcome is shown in the right panel of figure 13 as a gray-shaded band, overlaying the black line that represents our selected binning scheme as discussed in section 5. The red-shaded region shows the maximal variation when applying either the Hartlap correction or the Sellentin and Heavens modified likelihood, with the former reducing constraining power by approximately 10%, and the latter by about 1%.

Additionally, our results are influenced by the choice of galaxy bias, modeled as in eq. (2.6) and derived from the best-fit parameters of ref. [81]. To evaluate the sensitivity of our upper bound to variations in galaxy bias, we introduce a scaling factor b_g and re-define the bias as

$$b(z) = b_g \left[0.278 \left[(1+z)^2 - 6.565\right] + 2.393\right] . \tag{A.3}$$

Following [72], we adopt a uniform prior $b_g \in [0.1, 3.0]$. This scaling factor, being a constant multiplier of the final cross-correlation spectrum, is partially degenerate with the axion-photon coupling. Marginalizing over the full parameter space (mass, misalignment, and bias amplitude) results in a degradation of the achievable upper bound by approximately 0.3%. To illustrate the full variability of the result within the prior range for b_g, we show in the right panel of figure 13 the impact as a green shaded region. The smallest values of b_g degrade the bound by up to an order of magnitude, while the largest values improve the constraint by roughly half an order of magnitude.

JCAP06(2026)015

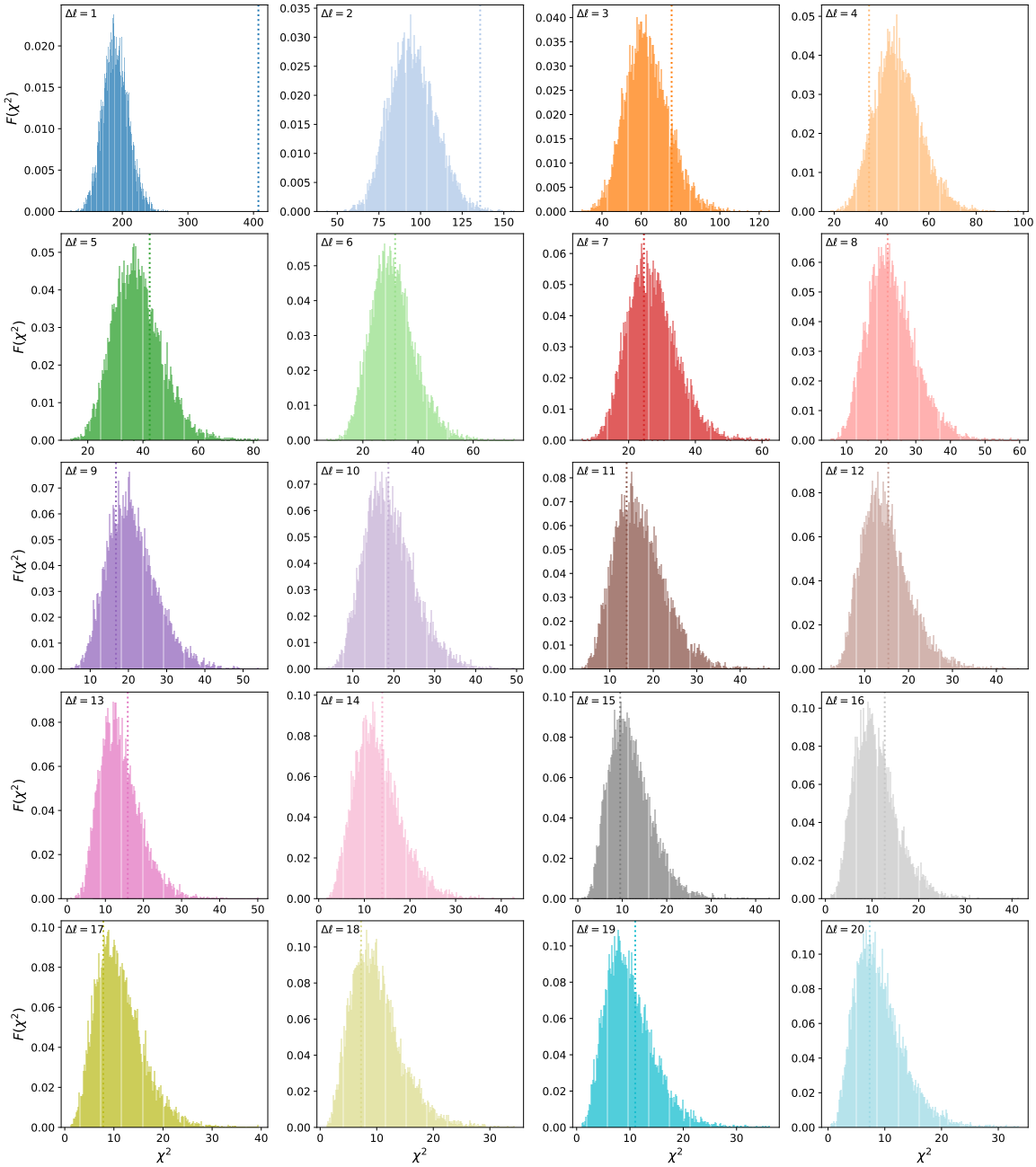


Figure 14. Chi-squared distributions for different binning bandwidths $\Delta\ell$, obtained from the 400 realizations. The vertical dotted lines indicates the χ^2 of data.

JCAP06(2026)015

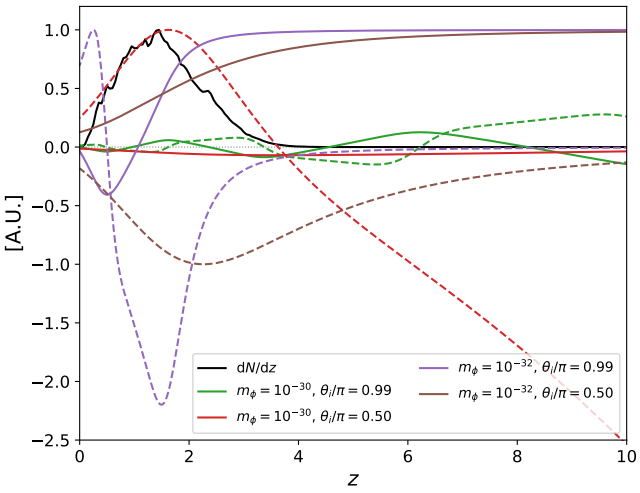


Figure 15. Redshift distribution of sources within the Quaia catalog in black and $\bar{\phi}$ (solid) and $\bar{\phi}'$ (dashed) for various values of the mass and the initial displacement.

B Galaxy distribution vs. scalar field evolution

As discussed in section 2, the spatial fluctuations of the scalar field are sourced by the metric perturbation h', which acts as an inhomogeneous forcing term on the field fluctuations, as shown in the right-hand side of eq. (2.4). Since h' is multiplied by the background (homogeneous) field derivative, $\bar{\phi}'$, the forcing term is suppressed when the field is frozen, while it is larger when the field is varying rapidly. The cosmological epoch at which the scalar field departs from its initial frozen state is controlled by its mass: the lighter the mass, the later the field starts its evolution. Figure 15 adds to the Quaia selection function the redshift evolution of the background field and its first derivative. For lower masses, a significant fraction of the field evolution occurs within the redshift range probed by Quaia, leading to an enhanced coupling.

References

[1] J.C. Mather et al., *A preliminary measurement of the Cosmic Microwave Background spectrum by the Cosmic Background Explorer (COBE) satellite*, *Astrophys. J. Lett.* **354** (1990) L37 [INSPIRE].

[2] W.C. Jones et al., *A measurement of the angular power spectrum of the CMB temperature anisotropy from the 2003 flight of BOOMERANG*, *Astrophys. J.* **647** (2006) 823 [astro-ph/0507494] [INSPIRE].

[3] WMAP collaboration, *Nine-year Wilkinson Microwave Anisotropy Probe (WMAP) observations: cosmological parameter results*, *Astrophys. J. Suppl.* **208** (2013) 19 [arXiv:1212.5226] [INSPIRE].

[4] Planck collaboration, *Planck 2013 results. XVI. Cosmological parameters*, *Astron. Astrophys.* **571** (2014) A16 [arXiv:1303.5076] [INSPIRE].

[5] Planck collaboration, *Planck 2015 results. XIII. Cosmological parameters*, *Astron. Astrophys.* **594** (2016) A13 [arXiv:1502.01589] [INSPIRE].

JCAP06(2026)015

[6] Planck collaboration, *Planck 2018 results. VI. Cosmological parameters*, *Astron. Astrophys.* **641** (2020) A6 [*Erratum ibid.* **652** (2021) C4] [arXiv:1807.06209] [INSPIRE].

[7] Planck collaboration, *Planck 2018 results. I. Overview and the cosmological legacy of Planck*, *Astron. Astrophys.* **641** (2020) A1 [arXiv:1807.06205] [INSPIRE].

[8] S.M. Carroll, G.B. Field and R. Jackiw, *Limits on a Lorentz and parity violating modification of electrodynamics*, *Phys. Rev. D* **41** (1990) 1231 [INSPIRE].

[9] S.M. Carroll, *Quintessence and the rest of the world*, *Phys. Rev. Lett.* **81** (1998) 3067 [astro-ph/9806099] [INSPIRE].

[10] D. Harari and P. Sikivie, *Effects of a Nambu-Goldstone boson on the polarization of radio galaxies and the cosmic microwave background*, *Phys. Lett. B* **289** (1992) 67 [INSPIRE].

[11] M. Li and X. Zhang, *Cosmological CPT violating effect on CMB polarization*, *Phys. Rev. D* **78** (2008) 103516 [arXiv:0810.0403] [INSPIRE].

[12] M. Pospelov et al., *Pseudoscalar perturbations and polarization of the cosmic microwave background*, *Phys. Rev. Lett.* **103** (2009) 051302 [arXiv:0808.0673] [INSPIRE].

[13] F. Finelli and M. Galaverni, *Rotation of linear polarization plane and circular polarization from cosmological pseudo-scalar fields*, *Phys. Rev. D* **79** (2009) 063002 [arXiv:0802.4210] [INSPIRE].

[14] K.R.S. Balaji, R.H. Brandenberger and D.A. Easson, *Spectral dependence of CMB polarization and parity*, *JCAP* **12** (2003) 008 [hep-ph/0310368] [INSPIRE].

[15] G.-C. Liu and K.-W. Ng, *Axion dark matter induced cosmic microwave background B-modes*, *Phys. Dark Univ.* **16** (2017) 22 [arXiv:1612.02104] [INSPIRE].

[16] L.M. Capparelli, R.R. Caldwell and A. Melchiorri, *Cosmic birefringence test of the Hubble tension*, *Phys. Rev. D* **101** (2020) 123529 [arXiv:1909.04621] [INSPIRE].

[17] R.R. Caldwell, V. Gluscevic and M. Kamionkowski, *Cross-correlation of cosmological birefringence with CMB temperature*, *Phys. Rev. D* **84** (2011) 043504 [arXiv:1104.1634] [INSPIRE].

[18] M. Galaverni, G. Gubitosi, F. Paci and F. Finelli, *Cosmological birefringence constraints from CMB and astrophysical polarization data*, *JCAP* **08** (2015) 031 [arXiv:1411.6287] [INSPIRE].

[19] E. Komatsu, *New physics from the polarized light of the cosmic microwave background*, *Nature Rev. Phys.* **4** (2022) 452 [arXiv:2202.13919] [INSPIRE].

[20] R.C. Myers and M. Pospelov, *Ultraviolet modifications of dispersion relations in effective field theory*, *Phys. Rev. Lett.* **90** (2003) 211601 [hep-ph/0301124] [INSPIRE].

[21] G. Gubitosi et al., *A constraint on Planck-scale modifications to electrodynamics with CMB polarization data*, *JCAP* **08** (2009) 021 [arXiv:0904.3201] [INSPIRE].

[22] G. Gubitosi, G. Genovese, G. Amelino-Camelia and A. Melchiorri, *Planck-scale modifications to electrodynamics characterized by a space-like symmetry-breaking vector*, *Phys. Rev. D* **82** (2010) 024013 [arXiv:1003.0878] [INSPIRE].

[23] V.A. Kostelecky and M. Mewes, *Lorentz-violating electrodynamics and the cosmic microwave background*, *Phys. Rev. Lett.* **99** (2007) 011601 [astro-ph/0702379] [INSPIRE].

[24] L. Caloni et al., *Probing Lorentz-violating electrodynamics with CMB polarization*, *JCAP* **03** (2023) 018 [arXiv:2212.04867] [INSPIRE].

[25] E. Witten, *Some properties of O(32) superstrings*, *Phys. Lett. B* **149** (1984) 351 [INSPIRE].

JCAP06(2026)015

[26] J.P. Conlon, *The QCD axion and moduli stabilisation*, *JHEP* **05** (2006) 078 [hep-th/0602233] [INSPIRE].

[27] P. Svrcek and E. Witten, *Axions in string theory*, *JHEP* **06** (2006) 051 [hep-th/0605206] [INSPIRE].

[28] A. Vilenkin and A.E. Everett, *Cosmic strings and domain walls in models with Goldstone and pseudoGoldstone bosons*, *Phys. Rev. Lett.* **48** (1982) 1867 [INSPIRE].

[29] M.C. Huang and P. Sikivie, *The structure of axionic domain walls*, *Phys. Rev. D* **32** (1985) 1560 [INSPIRE].

[30] R.L. Davis, *Cosmic axions from cosmic strings*, *Phys. Lett. B* **180** (1986) 225 [INSPIRE].

[31] A. Arvanitaki et al., *String axiverse*, *Phys. Rev. D* **81** (2010) 123530 [arXiv:0905.4720] [INSPIRE].

[32] D.J.E. Marsh, *Axion cosmology*, *Phys. Rept.* **643** (2016) 1 [arXiv:1510.07633] [INSPIRE].

[33] N. Kitajima, F. Kozai, F. Takahashi and W. Yin, *Power spectrum of domain-wall network, and its implications for isotropic and anisotropic cosmic birefringence*, *JCAP* **10** (2022) 043 [arXiv:2205.05083] [INSPIRE].

[34] M. Jain, A.J. Long and M.A. Amin, *CMB birefringence from ultralight-axion string networks*, *JCAP* **05** (2021) 055 [arXiv:2103.10962] [INSPIRE].

[35] L.F. Abbott and P. Sikivie, *A cosmological bound on the invisible axion*, *Phys. Lett. B* **120** (1983) 133 [INSPIRE].

[36] W. Lin and T.T. Yanagida, *Consistency of the string inspired electroweak axion with cosmic birefringence*, *Phys. Rev. D* **107** (2023) L021302 [arXiv:2208.06843] [INSPIRE].

[37] T. Fujita, K. Murai, H. Nakatsuka and S. Tsujikawa, *Detection of isotropic cosmic birefringence and its implications for axionlike particles including dark energy*, *Phys. Rev. D* **103** (2021) 043509 [arXiv:2011.11894] [INSPIRE].

[38] J. Preskill, M.B. Wise and F. Wilczek, *Cosmology of the invisible axion*, *Phys. Lett. B* **120** (1983) 127 [INSPIRE].

[39] M. Dine and W. Fischler, *The not so harmless axion*, *Phys. Lett. B* **120** (1983) 137 [INSPIRE].

[40] S. Nakagawa, F. Takahashi and M. Yamada, *Cosmic birefringence triggered by dark matter domination*, *Phys. Rev. Lett.* **127** (2021) 181103 [arXiv:2103.08153] [INSPIRE].

[41] I. Obata, *Implications of the cosmic birefringence measurement for the axion dark matter search*, *JCAP* **09** (2022) 062 [arXiv:2108.02150] [INSPIRE].

[42] R. Hlozek, D. Grin, D.J.E. Marsh and P.G. Ferreira, *A search for ultralight axions using precision cosmological data*, *Phys. Rev. D* **91** (2015) 103512 [arXiv:1410.2896] [INSPIRE].

[43] V. Poulin et al., *Cosmological implications of ultralight axionlike fields*, *Phys. Rev. D* **98** (2018) 083525 [arXiv:1806.10608] [INSPIRE].

[44] D. Kim et al., *Cosmic axion force*, *Phys. Rev. D* **104** (2021) 095010 [arXiv:2105.03422] [INSPIRE].

[45] A. Greco, N. Bartolo and A. Gruppuso, *Probing axions through tomography of anisotropic cosmic birefringence*, *JCAP* **05** (2023) 026 [arXiv:2211.06380] [INSPIRE].

[46] D. Gonzalez, N. Kitajima, F. Takahashi and W. Yin, *Stability of domain wall network with initial inflationary fluctuations and its implications for cosmic birefringence*, *Phys. Lett. B* **843** (2023) 137990 [arXiv:2211.06849] [INSPIRE].

JCAP06(2026)015

[47] S. Gasparotto and E.I. Sfakianakis, *Cosmic birefringence from the axiverse*, *JCAP* **11** (2023) 017 [arXiv:2306.16355] [INSPIRE].

[48] A. Greco, N. Bartolo and A. Gruppuso, *A new solution for the observed isotropic cosmic birefringence angle and its implications for the anisotropic counterpart through a Boltzmann approach*, *JCAP* **10** (2024) 028 [arXiv:2401.07079] [INSPIRE].

[49] V. Poulin, T.L. Smith, T. Karwal and M. Kamionkowski, *Early dark energy can resolve the Hubble tension*, *Phys. Rev. Lett.* **122** (2019) 221301 [arXiv:1811.04083] [INSPIRE].

[50] G. Choi, W. Lin, L. Visinelli and T.T. Yanagida, *Cosmic birefringence and electroweak axion dark energy*, *Phys. Rev. D* **104** (2021) L101302 [arXiv:2106.12602] [INSPIRE].

[51] K. Murai, F. Naokawa, T. Namikawa and E. Komatsu, *Isotropic cosmic birefringence from early dark energy*, *Phys. Rev. D* **107** (2023) L041302 [arXiv:2209.07804] [INSPIRE].

[52] S. Gasparotto and I. Obata, *Cosmic birefringence from monodromic axion dark energy*, *JCAP* **08** (2022) 025 [arXiv:2203.09409] [INSPIRE].

[53] M. Kamionkowski and A.G. Riess, *The Hubble tension and early dark energy*, *Ann. Rev. Nucl. Part. Sci.* **73** (2023) 153 [arXiv:2211.04492] [INSPIRE].

[54] S. Arcari et al., *Conversations in the dark: cross-correlating birefringence and LSS to constrain axions*, *JCAP* **10** (2024) 101 [arXiv:2407.02144] [INSPIRE].

[55] J.R. Eskilt et al., *Constraints on early dark energy from isotropic cosmic birefringence*, *Phys. Rev. Lett.* **131** (2023) 121001 [arXiv:2303.15369] [INSPIRE].

[56] H. Nakatsuka, T. Namikawa and E. Komatsu, *Is cosmic birefringence due to dark energy or dark matter? A tomographic approach*, *Phys. Rev. D* **105** (2022) 123509 [arXiv:2203.08560] [INSPIRE].

[57] T. Namikawa, *CMB mode coupling with isotropic polarization rotation*, *Mon. Not. Roy. Astron. Soc.* **506** (2021) 1250 [arXiv:2105.03367] [INSPIRE].

[58] Y. Minami and E. Komatsu, *New extraction of the cosmic birefringence from the Planck 2018 polarization data*, *Phys. Rev. Lett.* **125** (2020) 221301 [arXiv:2011.11254] [INSPIRE].

[59] T. Fujita, Y. Minami, M. Shiraishi and S. Yokoyama, *Can primordial parity violation explain the observed cosmic birefringence?*, *Phys. Rev. D* **106** (2022) 103529 [arXiv:2208.08101] [INSPIRE].

[60] P. Diego-Palazuelos et al., *Cosmic birefringence from the Planck data release 4*, *Phys. Rev. Lett.* **128** (2022) 091302 [arXiv:2201.07682] [INSPIRE].

[61] J.R. Eskilt, *Frequency-dependent constraints on cosmic birefringence from the LFI and HFI Planck data release 4*, *Astron. Astrophys.* **662** (2022) A10 [arXiv:2201.13347] [INSPIRE].

[62] A. Gruppuso, D. Molinari, P. Natoli and L. Pagano, *Planck 2018 constraints on anisotropic birefringence and its cross-correlation with CMB anisotropy*, *JCAP* **11** (2020) 066 [arXiv:2008.10334] [INSPIRE].

[63] M. Bortolami et al., *Planck constraints on cross-correlations between anisotropic cosmic birefringence and CMB polarization*, *JCAP* **09** (2022) 075 [arXiv:2206.01635] [INSPIRE].

[64] BICEP/KECK collaboration, *BICEP/Keck. XVII. Line-of-sight distortion analysis: estimates of gravitational lensing, anisotropic cosmic birefringence, patchy reionization, and systematic errors*, *Astrophys. J.* **949** (2023) 43 [arXiv:2210.08038] [INSPIRE].

[65] SPT collaboration, *Searching for anisotropic cosmic birefringence with polarization data from SPTpol*, *Phys. Rev. D* **102** (2020) 083504 [arXiv:2006.08061] [INSPIRE].

JCAP06(2026)015

[66] G. Zagatti et al., *Planck constraints on cosmic birefringence and its cross-correlation with the CMB*, *JCAP* **05** (2024) 034 [arXiv:2401.11973] [INSPIRE].

[67] A. Greco, N. Bartolo and A. Gruppuso, *Cosmic birefrigence: cross-spectra and cross-bispectra with CMB anisotropies*, *JCAP* **03** (2022) 050 [arXiv:2202.04584] [INSPIRE].

[68] PLANCK collaboration, *Planck intermediate results. LVII. Joint Planck LFI and HFI data processing*, *Astron. Astrophys.* **643** (2020) A42 [arXiv:2007.04997] [INSPIRE].

[69] M. Tristram et al., *Cosmological parameters derived from the final Planck data release (PR4)*, *Astron. Astrophys.* **682** (2024) A37 [arXiv:2309.10034] [INSPIRE].

[70] K. Storey-Fisher et al., *Quaia, the Gaia-unWISE quasar catalog: an all-sky spectroscopic quasar sample*, *Astrophys. J.* **964** (2024) 69 [arXiv:2306.17749] [INSPIRE].

[71] D. Alonso et al., *Constraining cosmology with the Gaia-unWISE quasar catalog and CMB lensing: structure growth*, *JCAP* **11** (2023) 043 [arXiv:2306.17748] [INSPIRE].

[72] G. Piccirilli et al., *Growth history and quasar bias evolution at $z < 3$ from Quaia*, *JCAP* **06** (2024) 012 [arXiv:2402.05761] [INSPIRE].

[73] GAIA collaboration, *Gaia data release 3: summary of the content and survey properties*, *Astron. Astrophys.* **674** (2023) A1 [arXiv:2208.00211].

[74] V. Gluscevic, D. Hanson, M. Kamionkowski and C.M. Hirata, *First CMB constraints on direction-dependent cosmological birefringence from WMAP-7*, *Phys. Rev. D* **86** (2012) 103529 [arXiv:1206.5546] [INSPIRE].

[75] T. Namikawa et al., *Atacama Cosmology Telescope: constraints on cosmic birefringence*, *Phys. Rev. D* **101** (2020) 083527 [arXiv:2001.10465] [INSPIRE].

[76] E. Di Dio, F. Montanari, J. Lesgourgues and R. Durrer, *The CLASSgal code for relativistic cosmological large scale structure*, *JCAP* **11** (2013) 044 [arXiv:1307.1459] [INSPIRE].

[77] J. Lesgourgues, *The Cosmic Linear Anisotropy Solving System (CLASS) I: overview*, arXiv:1104.2932 [INSPIRE].

[78] A. Challinor and A. Lewis, *The linear power spectrum of observed source number counts*, *Phys. Rev. D* **84** (2011) 043516 [arXiv:1105.5292] [INSPIRE].

[79] C. Bonvin and R. Durrer, *What galaxy surveys really measure*, *Phys. Rev. D* **84** (2011) 063505 [arXiv:1105.5280] [INSPIRE].

[80] M. Kamionkowski, J. Pradler and D.G.E. Walker, *Dark energy from the string axiverse*, *Phys. Rev. Lett.* **113** (2014) 251302 [arXiv:1409.0549] [INSPIRE].

[81] EBOSS collaboration, *Clustering of quasars in SDSS-IV eBOSS: study of potential systematics and bias determination*, *JCAP* **07** (2017) 017 [arXiv:1705.04718] [INSPIRE].

[82] D. Blas, J. Lesgourgues and T. Tram, *The Cosmic Linear Anisotropy Solving System (CLASS) II: approximation schemes*, *JCAP* **07** (2011) 034 [arXiv:1104.2933] [INSPIRE].

[83] A. Lue, L.-M. Wang and M. Kamionkowski, *Cosmological signature of new parity violating interactions*, *Phys. Rev. Lett.* **83** (1999) 1506 [astro-ph/9812088] [INSPIRE].

[84] M. Kamionkowski, *How to de-rotate the cosmic microwave background polarization*, *Phys. Rev. Lett.* **102** (2009) 111302 [arXiv:0810.1286] [INSPIRE].

[85] K.M. Górski et al., *HEALPix — a framework for high resolution discretization, and fast analysis of data distributed on the sphere*, *Astrophys. J.* **622** (2005) 759 [astro-ph/0409513] [INSPIRE].

JCAP06(2026)015

[86] T. Namikawa, *Tomographic constraint on anisotropic cosmic birefringence*, *Phys. Rev. D* **111** (2025) 023501 [arXiv:2410.05149] [INSPIRE].

[87] R.A. Sunyaev and Y.B. Zeldovich, *Small-scale fluctuations of relic radiation*, *Astrophys. Space Sci.* **7** (1970) 3 [INSPIRE].

[88] DES collaboration, *Quasar accretion disk sizes from continuum reverberation mapping in the DES standard-star fields*, *Astrophys. J. Suppl.* **246** (2020) 16 [arXiv:1811.03638] [INSPIRE].

[89] J. Kormendy and L.C. Ho, *Coevolution (or not) of supermassive black holes and host galaxies*, *Ann. Rev. Astron. Astrophys.* **51** (2013) 511 [arXiv:1304.7762] [INSPIRE].

[90] P.F. Hopkins et al., *A unified, merger-driven model for the origin of starbursts, quasars, the cosmic X-ray background, supermassive black holes and galaxy spheroids*, *Astrophys. J. Suppl.* **163** (2006) 1 [astro-ph/0506398] [INSPIRE].

[91] M.C. Powell et al., *The clustering of X-ray luminous quasars*, *Astrophys. J.* **891** (2020) 41 [arXiv:2001.07730].

[92] J.-F. Claeskens and J. Surdej, *Gravitational lensing in quasar samples*, *Astron. Astrophys. Rev.* **10** (2000) 263.

[93] M.A. DiPompeo, R.C. Hickox, S. Eftekharzadeh and A.D. Myers, *The characteristic halo masses of half-a-million WISE-selected quasars*, *Mon. Not. Roy. Astron. Soc.* **469** (2017) 4630 [arXiv:1705.05306].

[94] M. Rauch, *The Lyman alpha forest in the spectra of quasistellar objects*, *Ann. Rev. Astron. Astrophys.* **36** (1998) 267 [astro-ph/9806286] [INSPIRE].

[95] C. García-García et al., *The growth of density perturbations in the last ~ 10 billion years from tomographic large-scale structure data*, *JCAP* **10** (2021) 030 [arXiv:2105.12108] [INSPIRE].

[96] EBOSS collaboration, *The completed SDSS-IV extended Baryon Oscillation Spectroscopic Survey: BAO and RSD measurements from anisotropic clustering analysis of the quasar sample in configuration space between redshift 0.8 and 2.2*, *Mon. Not. Roy. Astron. Soc.* **500** (2020) 1201 [arXiv:2007.08998] [INSPIRE].

[97] B. Leistedt, H.V. Peiris and N. Roth, *Constraints on primordial non-Gaussianity from 800 000 photometric quasars*, *Phys. Rev. Lett.* **113** (2014) 221301 [arXiv:1405.4315] [INSPIRE].

[98] EBOSS collaboration, *Redshift-weighted constraints on primordial non-Gaussianity from the clustering of the eBOSS DR14 quasars in Fourier space*, *JCAP* **09** (2019) 010 [arXiv:1904.08859] [INSPIRE].

[99] SDSS collaboration, *Large scale clustering of Sloan Digital Sky Survey quasars: impact of the baryon density and the cosmological constant*, *Publ. Astron. Soc. Jap.* **57** (2005) 529 [astro-ph/0412631] [INSPIRE].

[100] EBOSS collaboration, *The clustering of the SDSS-IV extended Baryon Oscillation Spectroscopic Survey DR14 quasar sample: first measurement of baryon acoustic oscillations between redshift 0.8 and 2.2*, *Mon. Not. Roy. Astron. Soc.* **473** (2018) 4773 [arXiv:1705.06373] [INSPIRE].

[101] B.D. Sherwin et al., *The Atacama Cosmology Telescope: cross-correlation of CMB lensing and quasars*, *Phys. Rev. D* **86** (2012) 083006 [arXiv:1207.4543] [INSPIRE].

[102] B. Menard and M. Bartelmann, *Cosmological information from quasar-galaxy correlations induced by weak lensing*, *Astron. Astrophys.* **386** (2002) 784 [astro-ph/0203163] [INSPIRE].

[103] G. Risaliti and E. Lusso, *A Hubble diagram for quasars*, *Astrophys. J.* **815** (2015) 33 [arXiv:1505.07118] [INSPIRE].

JCAP06(2026)015

[104] D. Lang, *unWISE: unblurred coadds of the WISE imaging*, *Astron. J.* **147** (2014) 108 [arXiv:1405.0308].

[105] A.M. Meisner, D. Lang, E.F. Schlafly and D.J. Schlegel, *unWISE coadds: the five-year data set*, *Publ. Astron. Soc. Pac.* **131** (2019) 124504 [arXiv:1909.05444] [INSPIRE].

[106] E.L. Wright et al., *The Wide-field Infrared Survey Explorer (WISE): mission description and initial on-orbit performance*, *Astron. J.* **140** (2010) 1868 [arXiv:1008.0031] [INSPIRE].

[107] E. Hivon et al., *Master of the cosmic microwave background anisotropy power spectrum: a fast method for statistical analysis of large and complex cosmic microwave background data sets*, *Astrophys. J.* **567** (2002) 2 [astro-ph/0105302] [INSPIRE].

[108] D. Alonso et al., *Measurement of the power spectrum turnover scale from the cross-correlation between CMB lensing and Quaia*, *Open J. Astrophys.* **8** (2025) [arXiv:2410.24134] [INSPIRE].

[109] LSST Dark Energy Science collaboration, *A unified pseudo-C_ℓ framework*, *Mon. Not. Roy. Astron. Soc.* **484** (2019) 4127 [arXiv:1809.09603] [INSPIRE].

[110] D.A. Varshalovich, A.N. Moskalev and V.K. Khersonskii, *Quantum theory of angular momentum: irreducible tensors, spherical harmonics, vector coupling coefficients, 3nj symbols*, World Scientific, Singapore (1988) [DOI:10.1142/0270] [INSPIRE].

[111] M. Tegmark, *How to measure CMB power spectra without losing information*, *Phys. Rev. D* **55** (1997) 5895 [astro-ph/9611174] [INSPIRE].

[112] M. Tegmark and A. de Oliveira-Costa, *How to measure CMB polarization power spectra without losing information*, *Phys. Rev. D* **64** (2001) 063001 [astro-ph/0012120] [INSPIRE].

[113] J. Hartlap, P. Simon and P. Schneider, *Why your model parameter confidences might be too optimistic: unbiased estimation of the inverse covariance matrix*, *Astron. Astrophys.* **464** (2007) 399 [astro-ph/0608064] [INSPIRE].

[114] E. Sellentin and A.F. Heavens, *Parameter inference with estimated covariance matrices*, *Mon. Not. Roy. Astron. Soc.* **456** (2016) L132 [arXiv:1511.05969] [INSPIRE].

[115] Simons Observatory collaboration, *The Simons Observatory: science goals and forecasts*, *JCAP* **02** (2019) 056 [arXiv:1808.07445] [INSPIRE].

[116] LiteBIRD collaboration, *Probing cosmic inflation with the LiteBIRD cosmic microwave background polarization survey*, *PTEP* **2023** (2023) 042F01 [arXiv:2202.02773] [INSPIRE].

[117] CMB-S4 collaboration, *CMB-S4: forecasting constraints on primordial gravitational waves*, *Astrophys. J.* **926** (2022) 54 [arXiv:2008.12619] [INSPIRE].

[118] Euclid collaboration, *Euclid preparation. VII. Forecast validation for Euclid cosmological probes*, *Astron. Astrophys.* **642** (2020) A191 [arXiv:1910.09273] [INSPIRE].

[119] Euclid collaboration, *Euclid preparation. I. The Euclid wide survey*, *Astron. Astrophys.* **662** (2022) A112 [arXiv:2108.01201] [INSPIRE].

[120] DESI collaboration, *The DESI experiment, a whitepaper for Snowmass 2013*, arXiv:1308.0847 [INSPIRE].

[121] DESI collaboration, *The DESI experiment part I: science, targeting, and survey design*, arXiv:1611.00036 [INSPIRE].

[122] P. Diego-Palazuelos et al., *Robustness of cosmic birefringence measurement against galactic foreground emission and instrumental systematics*, *JCAP* **01** (2023) 044 [arXiv:2210.07655] [INSPIRE].

JCAP06(2026)015

[123] C. O'Hare, *cajohare/AxionLimits: AxionLimits*, https://cajohare.github.io/AxionLimits/ [DOI:10.5281/zenodo.3932430].

[124] M. Galaverni and F. Finelli, *Rotation of linear polarization plane from cosmological pseudoscalar fields*, *Nucl. Phys. B Proc. Suppl.* **194** (2009) 51 [INSPIRE].

[125] M. Galaverni, F. Finelli and D. Paoletti, *Redshift evolution of cosmic birefringence in CMB anisotropies*, *Phys. Rev. D* **107** (2023) 083529 [arXiv:2301.07971] [INSPIRE].

[126] X. Gan, L.-T. Wang and H. Xiao, *Detecting axion dark matter with black hole polarimetry*, *Phys. Rev. D* **110** (2024) 063039 [arXiv:2311.02149] [INSPIRE].

JCAP06(2026)015